Hydrodynamics of salt flat basins: the Salar de Atacama example

Marazuela, M.A.[a,b,c*]; Vázquez-Suñé, E.[a]; Ayora, C.[a]; García-Gil, A.[d]; Palma, T.[a,b,c]

[a] *Institute of Environmental Assessment and Water Research (IDAEA), CSIC, Jordi Girona 18, 08034 Barcelona, Spain*

[b] *Department of Civil and Environmental Engineering, Technical University of Catalonia (UPC), Jordi Girona 1-3, 08034 Barcelona, Spain*

[c] *Associated Unit: Hydrogeology Group (UPC-CSIC)*

[d] *Geological and Mining Institute of Spain (IGME), Manuel Lasala 44, 9° B, 50006 Zaragoza, Spain*

**Corresponding author. E-mail: mamarazuela@outlook.com*

KEYWORDS

Groundwater recharge, water balance, numerical model, saltwater intrusion, brine, lithium

HIGHLIGHTS

- A new regional groundwater flow for the Salar de Atacama was proposed.
- The hydrodynamics can be extended to other salt flat systems.
- The regional 3D numerical model served to validate the water balance.
- The conventional infiltration values for the hyperarid zones were not valid.
- Infiltration rates of hyperarid basin that reach 75 % are justified.

GRAPHICAL ABSTRACT

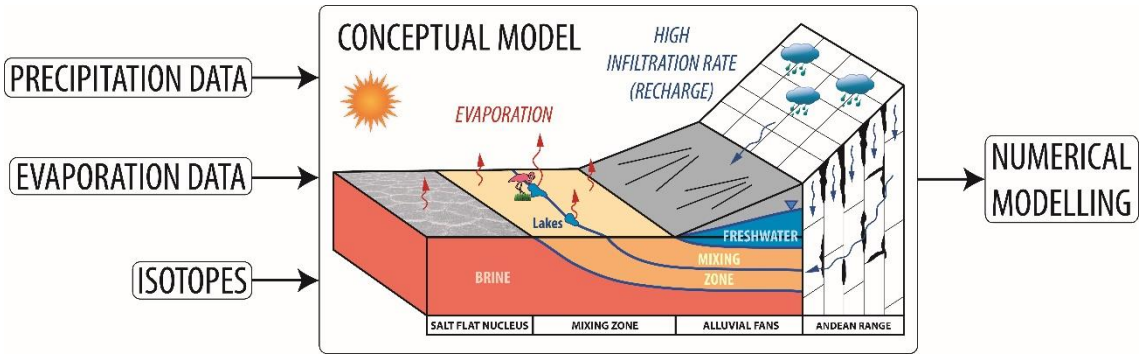

ABSTRACT

The Salar de Atacama is one of the most well-known saline endorheic basins in the world. It accumulates the world main lithium reserves and contains very sensitive ecosystems. The objective of this work is to characterize the hydrodynamics of the Salar de Atacama, and to quantify its complex water balance prior to the intense brine extraction. The methodology and results can be extrapolated to the groundwater flow and recharge of other salt flats. A three-dimensional groundwater flow model using low computational effort was calibrated against hundreds of hydraulic head measurements. The water infiltrated from the mountains ascends as a vertical flux through the saline interface (mixing zone) produced by the density contrast between the recharged freshwater and the evaporated brine of the salt nucleus. This water discharges and is largely evaporated from lakes or directly from the shallow water table. On the other hand, the very low hydraulic gradients, coupled with the presence of the mixing zone that operates as barrier, leads the salt flat nucleus to act as a hydrodynamically quasi-isolated area. The computed water table shows the lowest hydraulic head in the salt flat nucleus near the discharge at the mixing zone.

The groundwater balance of the Salar de Atacama in its natural regime was quantified resulting in an inflow/outflow of 14.9 $m^3 \cdot s^{-1}$. This balance considers the basin as an endorheic system. The very low infiltration values that are generally assumed for hyperarid basins are not consistent with the hydrogeology of the Salar de Atacama. Indeed, very high infiltration rates (up to 75% of rainfall) occur because of the high degree of fracturing of rocks and the scarce vegetation. This high infiltration is consistent with the light isotopic composition of the water from the recharge area (Altiplano). Therefore, the existence of additional inflows outside the basin is unlikely.

1. INTRODUCTION

Salt flats are saline and endorheic hydrogeological systems that are frequently associated with arid to hyperarid climates, in which the water table is several centimetres or decimetres below the ground surface. The largest salt flats in the world are on the Altiplano-Puna plateau of the Central Andean Range, which includes northwestern Argentina, southwestern Bolivia and north-eastern Chile (Risacher et al., 2003; Warren, 2010). The salt flats and their brines are a major source of lithium, boron, sodium chloride, iodine, potassium and magnesium (Evans, 1978; Kesler et al., 2012; Munk et al., 2016). Some of these elements are highly valued in the modern economy. For example, lithium is a main constituent in batteries for mobile phones, electric cars (Marom et al., 2011; Tarascon, 2010; Vikström et al., 2013) and even pharmacological treatments (Cipriani et al., 2005).

The Salar de Atacama (SdA) is the third largest salt flat in the world after the Salar de Uyuni (Bolivia) and Salinas Grandes (Argentina). Its brine contains a lithium concentration (~5,000 ppm) that is much higher than that of the other salt flats, and makes the SdA the main lithium reserve in the world. In addition, it is located in the most arid area of the Earth and houses exceptional ecosystems, such as the Reserva Nacional de los Flamencos (Ramsar site). These ecosystems are threatened because of the mining exploitation of the brine that has been occurring since the 1980s. In contrast, the brine pumping carried out have allowed to dispose of the best monitoring network in the world, which makes the SdA a reference for the scientific community.

The origin of the SdA dates to the Oligocene-Miocene boundary, synchronous with the increase in volcanic activity and Altiplano uplift (Arriagada et al., 2006). The uplift of the plateau marked the paleoclimatology history as a consequence of the strong topographic gradient reached, giving rise to a more humid plateau and a hyperarid salt flat (Rech et al., 2006). From this ancient time until the mid-1980s, the hydrodynamics of the system were controlled by the different climatic cycles. However, from the 1980s onward, the pumping of the brine for commercial purposes has altered its natural dynamics. Most of the studies that have been carried out in the SdA have analysed the current anthropogenic regime of the system (Salas et al., 2010), in which the water table of the salt flat has been drawn down. However, studies of the natural regime of the system, prior to exploitation, are lacking. Only the water table contour map of the eastern alluvial fans performed by HARZA (1978) is available. Unfortunately, this work does not take density differences into account.

Under the natural regime, the water table depth of the SdA was determined by a complex balance between the water inputs and outputs that tended to be zero (Rosen, 1994; Yechieli and Wood, 2002). The main recharge was precipitation (rainfall) that occurred in the mountains of the basin. The evaporation was controlled by the water table depth, which was a few decimetres below ground (Kampf et al., 2005; Kampf and Tyler, 2006; Tyler et al., 2006). The salt deposits accumulated because of the strong evaporation rates that were maintained for several thousands of years (Corenthal et al., 2016; Hardie, 1991; Wood and Sanford, 1990). These complex systems tend to be very sensitive to climatic and anthropogenic changes (Godfrey et al., 2013).

Although progress has been made in the last few decades to understanding the hydrogeology of the SdA, there are still many uncertainties in the water balance, and no water balance has been validated with numerical models. Thus, some authors present divergences about key factors to calculate the flow discharge: water table depth, areas of discharge and evaporation rates. The first study that addressed evaporation in the SdA (Mardones, 1986) quantified the volume of evaporated water as 5.29 $m^3 \cdot s^{-1}$. Assuming that in the basin-scale balance the inputs (recharge) are equal to the outputs (evaporation), this value should correspond to the recharge value. Subsequent works used this value as a reference and, obtained water balances in the range of 5.17-5.58 $m^3 \cdot s^{-1}$ (Dirección General de Aguas, 2013, 2010, 1986; Muñoz-Pardo et al., 2004). Kampf and Tyler (2006) obtained values of evaporation in a range of 1.6-22.7 $m^3 \cdot s^{-1}$, depending on the multiple calculation methods that were applied, which were based on remote sensing and evaporation zoning. Recently, Corenthal et al. (2016) used an approximated value of recharge from Bookhagen and Strecker (2008), applied the recharge model of Houston (2006) and obtained a net recharge of 0.9 $m^3 \cdot s^{-1}$ (26.5 $m^3 \cdot s^{-1}$ of rainfall with 3.5 % of infiltration). However, the same authors predicted that evaporation should have been 21.7 $m^3 \cdot s^{-1}$ to explain the amount of accumulated salts, and they proposed as a probable explanation that the estimated recharge deficit is compensated by contributions from the Altiplano outside the SdA basin. However, this approach is not consistent with the scarce presence of vegetation that would facilitate evapotranspiration and with the scarce evidence of surface runoff that would favour evaporation. If the evapotranspiration is very low and surface runoff almost non-existent, the recharge rate to aquifers should be very high. Therefore, there is still great uncertainty regarding the values of recharge and evaporation in the basin of the SdA under the natural regime.

Numerical models constitute a powerful tool to justify and validate the water balance. The steady-state models offer a hydrogeological reference for the system around which the system

will naturally oscillate. These models also serve as a basis to incorporate natural oscillations (e.g., cycles of evaporation, precipitation, etc.) and anthropogenic impacts (pumping and artificial recharge) in future transient-state models. However, determining the average water balance under the natural regime is not trivial and requires an analysis of a sufficiently large time interval that includes several dry and humid climatic cycles. In addition, three-dimensional (3D) numerical models represent a much more powerful tool than two-dimensional (2D) models as they allow to include recharge and evaporation processes within a geometry that faithfully reproduces the hydrostratigraphy of the basin in its three spatial components. This allows to quantify the total water balance at the basin scale.

The density contrast between the rainwater (freshwater) and the evaporated water (brine) results in a mixing zone (saline interface) that represents the dynamic equilibrium of both miscible fluids and has a strong influence on the groundwater flow (Marazuela et al., 2018) (Figure 1). To date, only 2D models of the mixing zone have been published in scientific manuscripts (Duffy and Al-Hassan, 1988; Fan et al., 1997; Holzbecher, 2005; Marazuela et al., 2018; Tejeda et al., 2003; Vásquez et al., 2013; Wooding et al., 1997). To the best of our knowledge, 3D numerical models that integrate the complex recharge-evaporation interaction within a salt flat do not exist. Moreover, no detailed studies have been conducted to provide a numerical response on a regional scale to the role that is played by the mixing zone and its lakes in a salt flat system. The principal reason for this lack of specific studies is probably the high computational cost and the absence of methodologies to consider the effects of density variations. In the case of the SdA, regional models have neglected the effects of density on the flow (Anderson et al., 2002; Muñoz-Pardo et al., 2004), despite of the large density contrasts (1 to 1.23 $kg \cdot L^{-1}$). To overcome this problem, Marazuela et al. (2018) proposed a methodology based on the correction of freshwater and mixed water heads by density variations in salt flats. This method allows the reproduction of the vertical flows that occur in the mixing zone at a low computational cost.

FIGURE 1

The objective of this study is to characterize the hydrogeological behaviour of the SdA and to quantify its complex water balance, prior to brine exploitation, to establish a reference for the salt flats studies. To reach the objective, firstly, the hydrogeological conceptual model of the system is defined and quantified to subsequently proceed to its 3D numerical modelling, which allows to validate the estimated water balance and to determine its uncertainties. The recent methodology proposed by Marazuela et al. (2018) for 3D numerical modelling of salt flats that

is based on the 3D mapping of the salt interface is used. This leads to a discussion about the recharge and hydrodynamics of the salt flat basins, and how the SdA basin can serve as a reference for the hydrogeological conceptualization of other salt flat basins and its 3D numerical modelling.

2. MATERIALS AND METHODS

The methodology followed in this work mixes experimental and numerical modelling techniques. First, it is performed a synthesis of the SdA location and its regional hydrodynamics, especially of its saline interface which was studied previously by Marazuela et al. (2018), and which serves as a basis for the correction of hydraulic heads by density variations applied in the 3D model of the present work. Second, the stratigraphy of the SdA focused on defining the geometry of the 3D numerical model is addressed. Third, the obtaining of experimental data such as precipitation and evaporation data, as well as the collection of isotope values that are included in the basin recharge discussion, is addressed. Fourth, the modelling strategies that are proposed for the salt flats modelling and which can be applied in the future to other analogous systems are defined. Fifth, all the characteristics of the 3D numerical model and the calibration are described.

2.1. STUDY AREA

The SdA basin, with a north-south elongated shape, is between 23° and 24° S latitude and 68° and 69° W longitude (Figure 2). To the east, it is enclosed by the main chain of the Andean Range (>5,500 m a.s.l., metres above sea level), while to the west, lies a secondary mountain range called the Cordillera de Domeyko. The salt flat, including the mixing zone, encompasses 3,000 km^2, and it is approximately 100 km in length and 50 km in width.

FIGURE 2

Four geomorphological zones from the depocenter to the watershed can be identified as follows: (1) salt flat nucleus; (2) mixing zone; (3) alluvial fans; and (4) volcanic and basement rocks (Figures 1 and 2). The salt flat nucleus is mainly made up of halite and it has an elevation of approximately 2,300 m a.s.l., whose topography exhibits a high level of roughness because of evaporation and ephemeral surface water. The mixing zone comprises calcite, gypsum and halite (Boschetti et al., 2007; Pueyo et al., 2017; Vásquez et al., 2013). The alluvial fans and particularly the volcanic and basement rock reach the highest altitude and constitute the main recharge area of the basin.

185 The hydrographic network is rather sparse and consists of two rivers, some streams and lakes;
186 most of the lakes are in the mixing zone. The main tributaries are the San Pedro and Vilama
187 Rivers, which originate to the north of the basin. Streams descend from the highest mountains
188 to disappear through infiltration in the highly permeable alluvial fans. The lakes are grouped
189 into four systems, namely, Soncor, which is feeded by the Burro Muerto channel, Aguas de
190 Quelana, Peine and Tilopozo (Figure 2). In addition, the Tebinquiche and the Cejar lakes can be
191 distinguished in the northern part of the San Pedro alluvial fan. The lakes have an extent of no
192 more than several hectares.

193 The exploitation of the brine is carried out in three plants constituted by evaporation pools,
194 where the pumped brine is transported. The pumping wells associated with the mining plant 1,
195 belonging to Albermale company, began in 1984 while those associated with mining plants 2
196 and 3, belonging to the Sociedad Química y Minera de Chile (SQM) company, began in 1994
197 and 1996, respectively.

198 *2.2. HYDROGEOLOGY OF THE SALINE INTERFACE (MIXING ZONE)*

199 The density contrast between the recharged rainwater (freshwater) and the evaporated water
200 (brine) results in a mixing zone (saline interface) that represents the dynamic equilibrium of
201 both miscible fluids and has a strong influence on the groundwater flow (Marazuela et al.,
202 2018) (Figure 1). The brine that is evaporated in the salt flat nucleus sinks because of gravity.
203 The sinking of the denser fluid causes the rise of less dense fluid. On the freshwater side of the
204 mixing zone, the groundwater that originates from the recharge area (mountains) is forced to
205 rise to the surface by the mixing zone because of its lower salinity. On the brine side of the
206 mixing zone, the brine also rises to the surface and is pushed by a convection cell that is similar
207 to the seawater intrusion process in coastal aquifers (Post and Werner, 2017; Werner et al.,
208 2013). Through this mechanism, the main discharge occurs in the freshwater-brine mixing
209 zone, where some lakes may appear, and the water table is very near the surface, which
210 results in higher evaporation rates (Cornellà et al., 2009; Tejeda et al., 2003).

211 Marazuela et al. (2018) differentiate three zones within the mixing zone depending on its
212 hydraulic characteristics: the internal mixing zone (IMZ) corresponds to the mixed water that is
213 pushed by the marginal convection cell of the nucleus and the middle mixing zone (MMZ) and
214 the external mixing zone (EMZ) are characterised by upward fluid flow from the mountains,
215 with high and medium flow velocities, respectively (Figure 1). This zoning is also evident on the
216 surface, and the corresponding lakes and wetlands are in the MMZ (Figure 2). The Los

Flamencos National Reserve occupies the northeastern and eastern mixing zone associated with the upward groundwater flow that provides the water to the lakes and wetlands.

2.3. STRATIGRAPHY OF THE SALAR DE ATACAMA

According to the lithological data of more than one thousand cores (IDAEA-CSIC, 2017; XTERRAE, 2011), with lengths that rang between less than 10 m and more than 200 m, six stratigraphic units can be distinguished in the salt flat nucleus as follows: (1) Unit A (Upper halite); (2) Unit AB (Upper gypsum with carbonates); (3) Unit B (Intermediate halite); (4) Unit C (Middle gypsums); (5) Unit D (Lower halite); and (6) Unit E (Clays) (Figure 3). The three upper hydrogeological units are of paramount importance for mineral resources and ecological sustainability, and these units are considered to be the main hydrological system. These layers constitute the more permeable area of the salt flat, the mineral exploitation domain, and they interact directly with the lakes of the mixing zone. Units C, D and E do not play any important hydrological role because of their lower permeability.

FIGURE 3

Furthermore, the stratigraphy of the SdA has been seriously affected by the synsedimentary tectonics, particularly by the Salar fault (Arriagada et al., 2006; Jordan et al., 2007; Mpodozis et al., 2005) but also slightly by the Tucúcaro fault (see their location in Figure 2). As a consequence, the thickness of the hydro-stratigraphic units has been affected and ranges from 50-250 m on the western side of the Salar fault to 400-500 m on the eastern side.

Unit A or aquifer A comprises pure halite with sediments and gypsum. Its porosity is higher than the underlying units. The sediments are clays, silts and sands of a brown to red colour. This unit is affected by the Salar fault; thus, in the western part, it has a thickness between 14 and 20 m, while in the eastern part, its thickness ranges between 25 and 40 m.

Unit AB or aquitard AB corresponds to a group of lithologies that present continuity through lateral facies changes, with a gradation from clays in the marginal zones to gypsum with carbonates in the nucleus. The thickness ranges between 0.2 m and 3 m, although in some areas it may be thicker.

Unit B or aquifer B comprises halite with sediments and gypsum in the western part. In the eastern part, the unit consists mainly of pure halite and lenses of organic matter and gypsum. In the western part, this unit has a variable thickness between 20 m and 25 m, while in the eastern part, the unit reaches up to 400 m in thickness.

2.4. EXPERIMENTAL DATA

A meteorological analysis was performed from January 1986 to December 2015. This interval was considered representative to stablish the average natural regime of the SdA basin as it includes several wet and dry cycles.

The rainfall study was based on the daily meteorological data that has been collected by 14 weather stations since the 1970s (see their location in Figure 4A). An interpolation that is consistent with the topography and meteorological data was performed for the average rainfall values of the basin. The interpolation of these meteorological data allowed to create the average isohyets map of the SdA for the 1986-2015 period (Figure 4A). Topographic factors were the dominant criterion for this interpolation. These estimated values may have a small uncertainty because not all of the weather stations records were continuous and complete, but in general, the amount and distribution of the data was considered good enough.

FIGURE 4

To quantify the recharge, the basin was discretized into 11 sub-basins and 30 zones (Figure 4). The sub-basin division was performed based on geomorphological and topographical features and watersheds. Each of these sub-basins captures the water that is recharged by rainfall in the mountains and moves it to the salt flat. In the salt flat and surroundings, the definition of zones was based on soil features. The recharge produced by rainfall infiltration was estimated subtracting the detention –defined below- from the total rained water in each rainfall event. One rainfall event comprises the integration of rainfalls that occurred in some consecutive days, mostly during the summer season. Detention is an equivalent term for the "initial abstraction" defined in the Runoff Curve Number methodology (Mishra and Singh, 2003) as the water held by interception, surface detention and infiltration at the beginning of a storm and that finally back to the atmosphere through evaporation. This detention value was applied to each event. Furthermore, previous $\delta^{18}O$ and $\delta^{2}H$ values of the groundwater of the SdA were used to discuss the location of its recharge (Huerta-Vásquez, 2012; Rissmann et al., 2015).

The potential evaporation data were obtained from the measurements that were taken at evaporation trays or evaporimeter tanks installed at the weather stations. Furthermore, several lysimeters collected evaporation data from the water table of the eastern mixing zone. The water table depth was the most critical factor in the evaporation rate in the SdA. Water table depth values were obtained from old reports and field campaigns (IDAEA-CSIC, 2017; Marazuela et al., 2018). To consider the depth of the water table, the methodology of Philip (1957) was used. This method correlates the evaporation value that is measured at the surface

with the water table depth through an exponential adjustment. The evaporation rate difference that is caused by solute concentration was directly included in the measurements. To quantify the evaporation flow, the zoning of Mardones (1986) was used as reference. This was slightly modified considering the new data and the availability of high-resolution satellite images, we improved this zoning (Figure 4C).

The stream flows was daily monitored by 15 gauging stations (see their location in Figure 2) during most of the analysed time. The missing data in the time series were filled with the average flow rate of each stream and were joined to the meteorological data of the weather stations and the ranges of oscillation in the nearby streams.

The hydraulic conductivity reference values were stablished considering previous studies and the interpretation of the pumping and packer test that was completed in the field by SQM. Over the last few decades, numerous scientific and technical studies have been conducted to assess the hydraulic properties of the study area (IDAEA-CSIC, 2017; Muñoz-Pardo et al., 2004; Rio Chilex S.A, 1997; Rockwood-Lithium, 2015). Furthermore, hydraulic tests, including packer tests, were conducted by SQM and then re-interpreted by the authors to obtain reference values. The parameter zoning (Figure 5) was based on geological features and pumping test results.

FIGURE 5

2.5. CRITERIA FOR THE 3D MODELLING OF THE MIXING ZONE OF SALT FLATS

2.5.1. Double boundary condition for modelling the mixing zone

Among the main difficulties in the modelling of salt flats is the presence of a freshwater-brine mixing zone within the modelled domain. In the similar case of coastal aquifers (Custodio and Bruggeman, 1987; Ferguson and Gleeson, 2012; Post et al., 2013; Post and Werner, 2017; Werner et al., 2013), the mixing zone is usually used as the outer boundary of the model and the sea level is prescribed. However, no numerical solution has been proposed for the regional modelling of the mixing zone of salt flats. In the available 2D numerical models of salt flats, almost the only ones made to date, two modelling strategies have been used: (1) reactive transport models taking into account evaporation and dissolution-precipitation processes (Hamann et al., 2015; Vásquez et al., 2013) and (2) to simplify the modelling strategies when the hydrochemical reactions are not the objective through the use of fixed hydraulic head in the saline interface (Duffy and Al-Hassan, 1988; Fan et al., 1997; Marazuela et al., 2018; Tejeda et al., 2003).

In the present work, the outflow from the mixing zone was treated by a double boundary condition (BC): (1) the main outflow was considered through the Neumann BC that is imposed in the entire surface mixing zone area as in the salt flat nucleus and (2) the rest of the outflow was considered through the Cauchy BC with the hydraulic head fixed along the MMZ. This methodology is valid as long as the mixing zone is not affected by pumping or strong perturbations. This option for modelling the saline interface is favoured for two reasons: the water table is fairly constant along the entire mixing zone that surrounds the salt flat nucleus, and this allows to close the total water balance with the balance component of greatest uncertainty. Although the evaporation of the salt flat nucleus and especially the recharge of each zone can be estimated and introduced to the model with high accuracy, the water that is ejected in the mixing zone may be more difficult to evaluate in the conceptual model because of the complex processes that occur in this area. In this approach, the balance can be reliably closed and adjusted to reality if the other calculations for recharging and evaporation have been correctly estimated. In addition, the boundary of the model must be located far enough from the mixing zone, being an efficient choice the contact between the alluvial fans and the basement, where the permeability is markedly reduced.

2.5.2. Hydraulic head corrections for density variations

Because of the presence of two miscible fluids of different density, i.e., freshwater and brine, the hydraulic heads that refer to each of the fluids cannot be co-modelled at a constant density without applying a correction, since the resulting groundwater flow would not be representative of reality (Maas and Emke, 1989; Oude-Essink, 2001; Strack, 1976). In coastal aquifers, where the area of interest is the land side (freshwater side), the seawater heads may be corrected to freshwater heads (Lusczynski, 1961; Post et al., 2007). Nevertheless, because the salt flat nucleus and its mixing zone are the areas of greatest interest, Marazuela et al. (2018) proposed to correct the fresh and mixed water heads to brine heads. This methodology was based on the 3D mapping of the regional mixing zone of the SdA, and the equations for the correction in each type of well are shown in detail there.

Thus, the hydraulic head data were corrected for variable density effects following the methodology proposed by Marazuela et al. (2018). A correction of the fresh and mixed water heads was applied to compensate for density variations, using the brine density, 1.23 $kg \cdot L^{-1}$, as reference. Thus, the water head of the observational points in the salt flat nucleus or very near it did not require any correction. The hydraulic heads that were measured in the mixing zone generally required a small compensation because the saline interface is very near the surface.

346 The hydraulic heads of the observational points in the alluvial and recharge zones required a
347 greater correction because the interface is deeper. The depth of screening and the local
348 stratigraphy were analysed as thoroughly as possible for each well.

349 The result of this hydraulic head correction is the existence of a regional minimum water head
350 in the mixing zone or near it. If this correction was not applied to the hydraulic heads, the
351 minimum piezometric head would be displaced to a more central position within the salt flat
352 nucleus. Then, the flow pathways would cross the mixing zone without considering the effects
353 of the variable density that drives an ascending flow in this area and feeds the lake
354 ecosystems. Alternatively, if the correction is applied, a minimum piezometric head is reached
355 in this area and reproduces the upward flow in the marginal zone at a low computational cost.

356 ## 2.6. NUMERICAL MODELLING

357 ### *2.6.1. Model set-up*

358 A steady-state model was built to reproduce the average water table of the natural regime of
359 the SdA and to justify the water balance before intensive brine extraction. The steady-state
360 flow equation was solved with the FEFLOW code (Diersch, 2014).

361 The model domain (see location Figure 2) encompassed an area of 3,303 km^2, which included
362 the nucleus, mixing zone and alluvial fans, and its bounds were defined on the basis of
363 hydrogeological features. The northern boundary corresponded to a structural lineament of
364 the basement, the eastern and southern boundaries largely represented the contact between
365 alluvial fans or the salt flat nucleus with the basement and volcanic rocks, and the western
366 boundary was the limit between the nucleus and the Cordillera de la Sal.

367 A 3D domain was used to model the regional groundwater flow of the SdA because a vertical
368 component of the flux and a vertical heterogeneity were identified. The three upper
369 hydrogeological units were considered: unit A is a free aquifer, unit AB is an aquitard, and unit
370 B acted as a semi-confined aquifer. The geometry of the hydrostratigraphic units was provided
371 by the correlation of cores and geophysical data (IDAEA-CSIC, 2017). Figure 6 shows the
372 geometry and topography of each geological unit.

373 **FIGURE 6**

374 The finite element mesh consisted of 168,025 nodes that were, arranged in 266,340 triangular
375 prismatic elements of variable size, and were distributed in four layers (Figure 7). Aquifer A
376 and aquitard AB were represented with one layer each one. Aquifer B was represented by two

finite element layers to smooth the mesh in the strong jump of the Salar fault. As a consequence, the south-western part of the bottom layer was deactivated. The grid was refined in the areas of greatest interest, such as the mixing zone and lakes.

FIGURE 7

2.6.2. Boundary conditions (BCs)

The inflows (the surface recharge, lateral groundwater recharge, streams and Soncor lake system) and outflows (evaporation) of the model were implemented by using several BCs as described below.

Surface recharge was applied in each zone of the domain through a Neumann BC (Figure 4C).

A fixed flow rate condition was applied to the lateral groundwater recharge and streams. The lateral recharge of each sub-basin was applied to the nodes of Unit B, which represented the groundwater flow that originates from the recharge occurring outside the model domain (Figure 4B). Only the North Alluvial and North Mixing Zone areas were applied to Unit A. The flow rates of the Jerez, Aguas Blancas, Talabre, Camar, Socaire, Peine and Tilomonte streams (their locations are shown in Figure 2) were fixed in the nodes of the Unit A, except for the Jerez stream. The San Pedro and Vilama Rivers and the Jerez stream were included in the lateral recharge value of the North Alluvial and North Mixing Zone areas.

A special case of recharge occurred in the complex Soncor lake system. The historical data of the water table showed a constant inter-annual hydraulic head of 2,300 m a.s.l. (with oscillations of only ± 0.1 m). This value was chosen to fit (Cauchy BC) the hydraulic head in Soncor lake system (Figure 4C).

The evaporation was treated with two BCs. On the one hand, for each defined zone of the salt flat nucleus and the mixing zone, an evaporation rate was imposed. On the other hand, part of the evaporation that occurs in the mixing zone was represented by a Cauchy BC along the MMZ (Figure 4C). The fixed water head was 2,299.9 m a.s.l., which corresponds to the average value in the mixing zone, and it was fairly constant during the considered time. The northern stretch of the mixing zone mapped in Figure 2 was not taken into account for the Cauchy BC (Figure 4C) because its hydraulic heads considerably changed with respect to the nucleus and the eastern mixing zone. The outflow from this zone was considered in the calibrated value of the Neumann boundary condition.

2.6.3. Model calibration

The mean of the hydraulic head value of the historical series at each observational point from January 1986 to December 1994 were used in the calibration. These values were corrected for density variations (see section 2.5.2). The data closest to Mining Plant 3 (see their location in Figure 2) were not considered because they were already affected by small local pumping during this period of time. Furthermore, the measurements of the hydraulic head measured since January 1995 were included only if they did not show perturbations due to mining activities. These observational points were mainly in the mixing zone and alluvial fans, far from the mining exploitation area, and they contributed to improve the calibration in the areas where no data prior to 1994 were available. Thus, a total of 299 observational points were used in the model calibration (Figure 2).

The lateral groundwater recharge was calibrated manually, while the evaporation rates for each zone and the hydraulic conductivities (K_x, K_y and K_z) were calibrated through steady-state inverse modelling with the parameter estimation code PEST (Doherty, 2015). The core of the PEST engine is the GLMA search algorithm, which iteratively optimizes the model parameters to improve its fit to observed data.

3. RESULTS

3.1. HYDROGEOLOGICAL BEHAVIOUR

The SdA is an endorheic basin in which the inputs correspond to the recharge that is produced by rainfall, and the outputs are represented by the evaporation that is produced from the salt flat nucleus and particularly in the surface mixing zone (Figure 8).

The Andean Range acts as a barrier to the cold Humboldt Current of the Pacific coast. Because it is under a subtropical high pressure zone, the SdA has a hyperarid climate, with low precipitation (Bookhagen and Strecker, 2008; Garreaud et al., 2010; Hartley and Chong, 2002). The main recharge is produced in the eastern side of the basin, in the Altiplano, particularly during the austral summer when the main rainfall events occur and particularly during wetter La Niña (ENSO) years. The water that is recharged in the mountains arrives mainly to the salt flat through lateral groundwater flow. When the lateral groundwater reaches the brine, it ascends to the surface as forced by the mixing zone, where a mixing and flow that is dominated by convection processes occur. Only a small portion of the recharge occurs through direct rainfall events on the salt flat or through the infiltration of water from rivers and streams.

The individualized results of the recharge, evaporation, streams and hydraulic parameters that characterize the SdA basin are described in detail below.

FIGURE 8

3.1.1. Recharge

The resulting isohyet map shows that precipitation in the highlands of the Andean Range exceeds 160 $mm \cdot yr^{-1}$, while in the salt flat nucleus, precipitation barely reaches 10 $mm \cdot yr^{-1}$. The most western area of the basin show precipitation values of less than 5 $mm \cdot yr^{-1}$. Therefore, the SdA basin exhibits precipitation values that are typical of hyperarid zones, while in the mountains, the rainfall rates are much higher.

There are no experimental works that quantify the values of detention in the Atacama region. The high degree of fracturing of the ignimbrites and volcanic rocks in the mountains (recharge area) and the predominant coarse-grained composition of the alluvial fans results in a little developed surface runoff and a very high infiltration. Additionally, the sparse vegetation also contribute to very low evapotranspiration from the soil. Some direct observations in several piezometers of the salt flat show that rainfall events of less than 5 mm do not produce any response in the groundwater heads (Figure 9). This value was selected as representative of the detention in the salt flat; it was also extrapolated for the entire basin in the absence of previous experimental data on the recharge in the mountains and it was based on the previous criteria (sparse vegetation and a high degree of fracturing). After detracting 5 mm from the rainfall, the estimated detention for the sub-basins was between 25 % and 85 % (Table 1), and for the zones of the salt flat and surroundings, this value was 35 % (Table 2).

FIGURE 9

TABLE 1

TABLE 2

Therefore, the calculated average precipitation in the SdA basin was 23.5 $m^3 \cdot s^{-1}$, and the recharge (precipitation minus detention) to the aquifers was 16.2 $m^3 \cdot s^{-1}$. The precipitation value is quite reliable and it is only submitted to the small uncertainty of the interpolation technique. The recharge estimation has a somewhat greater uncertainty because the exact detention is more difficult to quantify.

3.1.2. Evaporation

According to the data that were collected at the different weather stations, the average annual temperature was 14 °C, with a maximum of 24 °C during February (summer) and a minimum of 4 °C during July (winter).

The measurements show an annual evaporation rate that oscillates between 1,100 $mm \cdot yr^{-1}$ and 4,500 $mm \cdot yr^{-1}$. The variation was attributed to the seasonal behaviour of the potential evaporation. These potential values of evaporation decrease exponentially until they disappear when the water table reaches depths between 0.5 and 2 m.

The evapotranspiration that was produced by vegetation was neglected because the surface that is covered by vegetation is less than 5 %; it is also not a continuous and dense cover, which makes it difficult to predict with traditional methods. Therefore, taking into account the depth of the water table and integrating the different evaporation zones (Figure 4C), the total discharge of water by evaporation in the studied area was initially estimated in 16.0 $m^3 \cdot s^{-1}$. This result is significantly larger than the discharge of 5.0 to 6.0 $m^3 \cdot s^{-1}$ obtained by Mardones (1986), that has been used as reference in many water mass balances up to now (Dirección General de Aguas, 2013, 2010, 1986) . Nevertheless, using the original Mardones' exponential curves and the groundwater depth data obtained from old reports and surveys, the discharge results in 15.0 $m^3 \cdot s^{-1}$ (HARZA, 1978; Marazuela et al., 2018; Rio Chilex S.A, 1997), a value close that obtained in the present study.

3.1.3. Streams

The surface drainage network develops from the highlands to the salt flat during intermittent rainy periods. The water that originates from the rainfall in the mountains moves downhill until it disappears through infiltration in the alluvial fans. These drainages are in the northern and eastern areas of the basin. The average value of each stream is shown in Table 3. The highest flows are in the San Pedro and Vilama Rivers, with average values of 0.72 $m^3 \cdot s^{-1}$ and 0.28 $m^3 \cdot s^{-1}$, respectively. The flow of the eastern streams ranges between 0.15 $m^3 \cdot s^{-1}$ and 0.01 $m^3 \cdot s^{-1}$.

TABLE 3

3.1.4. Hydraulic parameters

The evaporites and cemented detrital materials of the salt flat nucleus and the mixing zone have a low hydraulic conductivity. However, the karstification that occurs because of dissolution can increases these values by several orders of magnitude, which results in preferential underground channels (Bakalowicz, 2005). In a simplified manner, these materials

can be treated as a discretized equivalent porous media (Scanlon et al., 2003). The hydraulic test performed in the nucleus showed transmissivities between almost zero to more than 10,000 $m^2 \cdot d^{-1}$. In the case of the alluvial fans, the hydraulic tests show transmissivity values from 2,000 $m^2 \cdot d^{-1}$ to 9,000 $m^2 \cdot d^{-1}$. The reference hydraulic conductivity values are shown in Table S1.

3.2. GROUNDWATER FLOW DYNAMICS

The hydraulic head contour map that was obtained from the natural steady-state model is shown in Figure 10. The fit of the observational data to the simulation data is expressed through the objective function (the weighted sum of the squares of the residuals between the observations and the simulation results). The results of the hydraulic head calibration are shown in Figure 11, and the lateral recharge, superficial recharge and hydraulic conductivity values that were obtained are shown in Tables 1, 2 and S1, respectively. The results show a very accurate fit of the data with an average error of 0.48 m and a root mean square and a standard deviation of 0.64 m. The errors of the model are not spatially concentrated which indicate that the calibration is accurate for all model zones.

FIGURE 10

FIGURE 11

The resulting water table is representative of the average climate under natural regime. Therefore, this is the water table around which the hydraulic heads oscillates due to natural perturbations (e.g., rainfall events or evaporation cycles).

The hydraulic gradients cause the flow to converge from the mountains to the mixing zone and to the eastern and south-eastern area of the salt flat nucleus. Higher hydraulic gradients are identified in the northern, eastern and southeastern zones, which coincides with the main lateral recharge sub-basins. The lower hydraulic gradients occur in the salt flat nucleus because of the low rainfall, flat topography and high hydraulic conductivities. The specific characteristics of each zone defined in Figure 10 and are described as follows.

In the northwestern sector of the domain (Zone 1 of Figure 10), groundwater flows from the northeast to the southwest in its northernmost zone, which gives way to a north-south flow and finally to a northwestern-southeastern flow in the San Pedro alluvial fan. The hydraulic heads oscillate between 2,340 m a.s.l. in the north and up to 2,300 m a.s.l. near the nucleus. Of particular importance are Tebinquiche and Cejar lakes (their locations are shown in Figure 2)

that constitute the relative minimum piezometric heads and act as local discharge zones through evaporation.

In the northeastern sector (Zone 2), groundwater flows from the northeast to the southwest. The flow follows to a great extent the geometry of the alluvial fans to their end at the mixing zone, where the hydraulic heads are approximately 2,300 m a.s.l. Zone 3 is the southward extension of the trend that is described in Zone 2 where the groundwater flow move in east-west direction, from the Andean Range to the mixing zone (Zone 6).

Zone 4 corresponds to the discharge of the Monturaqui aquifer (Anderson et al., 2002; Boutt et al., 2016; Rissmann et al., 2015). It shows more pronounced hydraulic gradients than in nearby areas, with a SE-NW flow direction and water heads that ranges from 2,316 m a.s.l. to 2,300 m a.s.l.

A sector of special interest because of its hydrogeological location and ecology is the Soncor lake system (Zone 5). This zone is characterized by water heads of approximately 2,300 m a.s.l. Although a great part of the water is evaporated, another part infiltrates aquifer A.

The regional minimum water head is located in the mixing zone or in the eastern and south-eastern part of the salt flat nucleus, near the mixing zone (Zone 6). An upward flow of freshwater from the eastern side discharges the mixing zone, as the vertical hydraulic gradients show in Figure 12. In addition, the brine from the nucleus also follows an upward flow in this area although with much lower hydraulic gradient.

FIGURE 12

The nucleus of the SdA (Zone 7) is characterized by very low hydraulic gradients, as in an area of approximately 1,360 km^2, the difference between the maximum and minimum hydraulic heads is barely 4 m. The western part of the nucleus presents somewhat higher gradients than the eastern part, particularly in the southwestern sector. The groundwater flows from southwest to northeast in the western sector. Once the flow path lines reach the eastern part of the nucleus, they continue to rotate toward southeast, where the regional minimum water head is reached.

3.3. WATER BALANCE

The water balance of the system was quantified through the numerical model in 14.9 $m^3 \cdot s^{-1}$ for both the inflows and outflows of the SdA basin, which leaves the net balance equal to zero (Figure 13).

FIGURE 13

The total recharge comprised lateral recharge from peripheral sub-basins (87.2 %), surface recharge that was produced by rainwater on the modelled domain (8.6 %), streams (2.2 %), and water that returned to the upper aquifer through infiltration from the Soncor lake system (2.0 %).

The total lateral recharge from the peripheral sub-basins was 13.0 $m^3 \cdot s^{-1}$. The main lateral recharge of the modelled domain was produced by the northern area that includes the Rio Grande and Toconao sub-basins, followed by the sub-basins of the Socaire, Monturaqui and Talabre; the least water was provided by the western sub-basins. Therefore, the main recharge was produced in the northern, eastern and south-eastern parts of the system, with very little lateral recharge from the western section because the heights of the western mountains are much smaller, and the mountains thus receive less precipitation.

The direct rainfall on the modelled area was much less than in the peripheral sub-basins because of its lower topography. However, the amount of water that was recharged was not negligible and reached 1.3 $m^3 \cdot s^{-1}$. The streams from the zones outside the domain also made a small contribution to the system, with a total of 0.3 $m^3 \cdot s^{-1}$.

A component of particular interest in the hydrodynamics of the system is the Soncor lake system. It collected water from the mixing zone. All of these water contributions converged in the Burro Muerto channel and later arrived at the different lakes of Soncor. The surface system ends up overflowing to the south of Barros Negros lake (the largest lake of Soncor) and, it constituted a water return of 0.3 $m^3 \cdot s^{-1}$ to aquifer A.

The outputs of the system were produced entirely through evaporation, with a total of 14.9 $m^3 \cdot s^{-1}$. The salt flat nucleus evaporated 0.9 $m^3 \cdot s^{-1}$, while the mixing zone evaporated a total of 14.0 $m^3 \cdot s^{-1}$. A part of the water that evaporated in the mixing zone corresponds to that was produced through the Neumann BC on the surface (9.7 $m^3 \cdot s^{-1}$), and another part corresponds to the water that was produced through the Cauchy BC in the MMZ (4.3 $m^3 \cdot s^{-1}$). The small inputs that were locally produced by the Cauchy BC are negligible.

4. DISCUSSION

As any endorheic basin, the water table of the SdA under natural regime is the result of the balance between the inputs that mainly occur in the highlands and the outputs that occur in the mixing zone and in the salt flat nucleus by evaporation. The recharge of the basin occurs mainly in the north, east and southeast parts of the basin where the highest topography is

595 reached. No external water entries were considered from outside the basin. The water table
596 was characterized by strong hydraulic gradients in the zones of higher topography and low
597 hydraulic gradients in the salt flat (Figure 10). As a consequence of the topography and the
598 geological features, the resulting water table evidences an asymmetry respect to the north-
599 south axis. The minimum hydraulic head is located in the mixing zone or in the eastern part of
600 the nucleus.

601 The main vertical groundwater flows that result from the 3D numerical model occurs in the
602 mixing zone or in the easternmost zone of the nucleus, near to the mixing zone where the
603 lower hydraulic head is located (Figures 10 and 12). The location of the regional piezometric
604 minimum in the eastern and southeastern sector of the nucleus, which was near the mixing
605 zone but not always in the mixing zone itself, may be due to the evaporation that occurs in the
606 nucleus of the salt flat under its natural regime. The water that reaches the mixing zone from
607 the mountains largely evaporates in the lakes of the mixing zone or directly from the water
608 table that is very shallow in this area (less than 1 m depth). Therefore, the eastern mixing zone
609 constitute the main outflow of the system. Another part of this upward water mixes with the
610 brine and reaches the nucleus because of the convection cell. This flow pattern is consistent
611 with the increase in densities in the nucleus from the eastern zone (1.18-1.20 $kg \cdot L^{-1}$) to the
612 west-central zone (1.23 $kg \cdot L^{-1}$). This consistency indicates that the regional flow that is
613 controlled by the variable density of the fluid was satisfactorily reproduced at a constant
614 density, which validates the methodology that was proposed by Marazuela et al., (2018) for
615 the numerical modelling of salt flats with low computational effort. The outflow produced
616 through the mixing zone reached 14.0 $m^3 \cdot s^{-1}$ what equals to 94 % of the total water balance
617 outputs. Only the 6 % of the outflow was produced through the salt flat nucleus in the natural
618 regime.

619 In the northeastern mixing zone, the presence of vertical fracturing planes favours the
620 upwelling of groundwater (Marazuela et al., 2018). This water that rises in the northeastern
621 mixing zone is channelled in part by the Burro Muerto channel and flows to the Soncor lake
622 system, which not only favours evaporation from the surface water but also generates a re-
623 entry of water into the aquifer through overflowing and infiltration. However, this mixing zone
624 was not mirrored in the western margin because of the presence of the Cordillera de la Sal,
625 made up of salt rocks, produces enrichment in salts. Therefore, this enrichment causes a
626 gradual increase in the density of the small amount of water (lower topography) that is
627 recharged in the western sector of the basin. As a consequence, the mixing zone was much
628 further to the west from the salt flat and possibly much more gradual.

629 The nearly absent hydraulic head gradients in the salt flat nucleus, coupled with the presence
630 of the saline interface that acts as a barrier on the eastern side, leads the salt flat nucleus to
631 act as quasi-isolated area, where the small flows that occur are induced by the density
632 contrasts. The main responsible for the low hydraulic gradients is the topography that
633 conditions the recharge and the strong karstification of the evaporitic materials. Due to the
634 karstification processes, the hydraulic conductivities obtained from the pumping tests and the
635 calibration of the numerical model for the equivalent porous medium was very high. This
636 barrier effect that is exerted by the saline interface could have a decisive influence on the
637 hydraulic response of the water table when a recharge or pumping event occurred between
638 the nucleus and the EMZ such as the events described by Boutt et al. (2016) in the
639 southeastern mixing zone.

640 The total water balance, which was estimated as 16.2 $m^3 \cdot s^{-1}$ for the rainfall recharge (section
641 3.1.1) and 16.0 $m^3 \cdot s^{-1}$ for the evaporation (section 3.1.2), was slightly higher than the water
642 balance that is obtained with the calibrated numerical model which was computed as 14.9
643 $m^3 \cdot s^{-1}$ for both of them. This small difference (<8 %) corresponds mainly to a reduction in the
644 lateral recharge from the Monturaqui sub-basin during the calibration process. In this sub-
645 basin, the shortage of weather stations prevented a more detailed isohyetal mapping of the
646 zones of greater precipitation. Therefore, the recharge water could be slightly overestimated
647 in the initial conceptual model.

648 The water balance studies that have been conducted by the Chilean government (Dirección
649 General de Aguas, 2013, 2010, 1986) and researchers (Muñoz-Pardo et al., 2004) have used as
650 reference the 5.29 $m^3 \cdot s^{-1}$ value estimated by Mardones (1998). This value is much less than the
651 value that was obtained from our study (16.0 $m^3 \cdot s^{-1}$). Nevertheless, using the original
652 Mardones' exponential curves and the groundwater depth data obtained from old reports and
653 surveys, the discharge results in 15.0 $m^3 \cdot s^{-1}$ (HARZA, 1978; Marazuela et al., 2018; Rio Chilex
654 S.A, 1997), a value close that obtained in the present study.

655 On the other hand, according to the later estimation of Kampf and Tyler (2006), the discharge
656 could reach 22.7 $m^3 \cdot s^{-1}$. Corenthal et al. (2016) estimated a long-term discharge rate of 21.7
657 $m^3 \cdot s^{-1}$ to explain the accumulation of halite deposits. According to our water table depths data
658 and considering the application of the Philip (1957) fitting curve, the evaporation that was
659 obtained for the salt flat is reasonable and the main controversy is the infiltration rate
660 considered in each case. The same authors estimated the gross recharge as 26.5 $m^3 \cdot s^{-1}$ based
661 on the TRMM 2B31 data set of Bookhagen and Strecker (2008). Our specific recharge study

slightly refined this value to 23.5 $m^3 \cdot s^{-1}$. This shows the high sensitivity of the evaporation with the water table depth and the need of its accurate measurements in endorheic basin studies.

The main discussion to estimate the amount and location of the recharged water is the infiltration rate. Traditionally, it has been assumed that the infiltration rate in arid to hyperarid zones is very low, with values that can range between 0.1-5 %, with the most part being evaporated from the soil (Scanlon et al., 2006). Following this common assumption, Corenthal et al. (2016) concluded that an infiltration rate of 3 %, which was obtained by applying the Houston (2009) recharge model, would results in an effective recharge of only 0.9 $m^3 \cdot s^{-1}$ and cannot explain the amount of halite that has accumulated in the basin. According to these authors, a possible explanation would be a much wider recharge area from the Altiplano towards the SdA basin. However, this hypothesis assumes that most of the recharge occurs from outside the basin, and there is no clear evidence of this. In addition, this hypothesis would imply that the water that recharges the SdA from the Altiplano would have relatively heavy $\delta^{18}O$ and $\delta^{2}H$ values because of the low infiltration and high evaporation rates is assumed by these authors and the presence of numerous salt flats in the Altiplano.

In contrast, we assumed in our model that most of the rainfall infiltrates with a minor fraction being evaporated from the soil. Indeed, the main recharge zone comprises ignimbrites, lava flows and different basement rocks. All these rocks evidence a low degree of incision by superficial hydric erosion, which indicates that most of the rainwater infiltrates preventing its rapid evaporation. The sparse vegetation in these zones neither favours evapotranspiration from the soil. In addition, all these rocks are strongly affected by fractures and deep grooves because of tectonics and the cooling process of volcanic rocks. A high infiltration rate (i.e., low detention) is also consistent with the isotopic values of the recharge water. The $\delta^{18}O$ and $\delta^{2}H$ values of the groundwater from the wells and boreholes of the eastern and southeastern recharge area of the SdA, prior to the mixing zone, plot very close to the Local Meteoric Water Line, and show nearly no evaporation (Figure 14). This result is also consistent with the isotopic values of Herrera et al. (2016), which show exactly the same characteristics in an area (Laguna Tuyajto) of the Altiplano several kilometres to the east of the watershed of the SdA. Only one of the samples that was analysed by these authors showed evidences of evaporation, but they explained it as a sample that was taken from nearly still water in a small pond. Therefore, all these reasons indicate that rainwater quickly infiltrate, without sufficient time to evaporate. In addition, this result disprove the presence of evaporated primary water flows from the other salt flats of the Altiplano (outside the basin) as the main source of the enriched

elements in the brine, which is in any case, a very specific process and scarcely important at a regional scale.

FIGURE 14

For all these reasons, it can be inferred that the infiltration rates of 0.1-5 % that are traditionally associated with hyperarid systems, with evaporation rates of less than 35 $mm \cdot yr^{-1}$ in many cases, are not applicable to the SdA basin where the topography reaches 5,000 m a.s.l., with precipitation rates of 160 $mm \cdot yr^{-1}$ (Figure 4A).

5. SYNTHESIS AND CONCLUSIONS

The regional groundwater flow and the complex water balance of the SdA under its natural regime, previous to mining exploitation, were characterized and quantified. A three-dimensional groundwater flow model was used to assess the coherence of the water balance. The model uses a low computational effort method based on hydraulic head corrections by density variations to reproduce the vertical fluxes of the mixing zone (saline interface) in salt flats.

The recharge of the system occurs mainly in the north, east and southeast sub-basins where the highest elevations are reached. The lowest hydraulic head is located near the eastern mixing zone. Thus, the mixing zone constitutes the main outflow of the system and it is motivated by the vertical hydraulic gradients. The groundwater flow that reaches the mixing zone from the mountains is largely evaporated in both, the lakes of the mixing zone or directly from the shallow water table. The nearly absent hydraulic gradients in the salt flat nucleus, coupled with the presence of the mixing zone that operate as barrier lead the salt flat nucleus to act as a hydrodynamically quasi-isolated area. This is a general trend that can be expected in the hydrodynamics of any salt flat system.

The basin water balance was quantified as 14.9 $m^3 \cdot s^{-1}$ in natural regime for both, the inflows and outflows. The water balance considered the basin as an endorheic system which was consistent with the isotopic data. The very low infiltration values that are generally assumed for hyperarid basins are not consistent with the hydrogeology of the SdA and very high infiltration rates occur because of the high degree of fracturing of rocks and the scarce vegetation. The existence of evaporated inflows from the Altiplano (outside the basin) as the main source of the enriched elements in the brine therefore seems to be unlikely. This behaviour of the recharge in the SdA basin with high infiltration rates in hyperarid climates, should serve as reference for future studies in other continental saline systems of the world.

This is also of great importance to know the origin and renewal rate of chemical elements that are extracted from the salt flat brines.

ACKNOWLEDGMENTS

The authors acknowledge Sociedad Química y Minera de Chile S.A. (SQM) for their support and sharing data throughout the hydrogeological characterization of the SdA site. M.A. Marazuela gratefully acknowledges the financial support from the AGAUR (Agència de Gestió d'Ajuts Universitaris I de Recerca, Generalitat de Catalunya) and the European Union (grant number 2017FI B1 00194). Finally, we thank three anonymous reviewers for their valuable comments.

753 **REFERENCES**

754 Anderson, M., Low, R., Foot, S., 2002. Sustainable groundwater development in arid, high
755 Andean basins. Geol. Soc. London, Spec. Publ. 193, 133–144.

756 Aravena, R., Suzuki, O., Peña, H., Pollastri, A., Fuenzalida, H., Grilli, A., 1999. Isotopic
757 composition and origin of the precipitation in Northern Chile. Appl. Geochemistry 14,
758 411–422. doi:10.1016/S0883-2927(98)00067-5

759 Arriagada, C., Cobbold, P.R., Roperch, P., 2006. Salar de Atacama basin: A record of
760 compressional tectonics in the central Andes since the mid-Cretaceous. Tectonics 25,
761 TC1008. doi:10.1029/2004TC001770

762 Bakalowicz, M., 2005. Karst groundwater: A challenge for new resources. Hydrogeol. J. 13,
763 148–160. doi:10.1007/s10040-004-0402-9

764 Bookhagen, B., Strecker, M.R., 2008. Orographic barriers, high-resolution TRMM rainfall, and
765 relief variations along the eastern Andes. Geophys. Res. Lett. 35, L06403.
766 doi:10.1029/2007GL032011

767 Boschetti, T., Cortecci, G., Barbieri, M., Mussi, M., 2007. New and past geochemical data on
768 fresh to brine waters of the Salar de Atacama and Andean Altiplano, northern Chile.
769 Geofluids 7, 33–50. doi:10.1111/j.1468-8123.2006.00159.x

770 Boutt, D.F., Hynek, S.A., Munk, L.A., Corenthal, L.G., 2016. Rapid recharge of fresh water to the
771 halite-hosted brine aquifer of Salar de Atacama, Chile. Hydrol. Process. 30, 4720–4740.
772 doi:10.1002/hyp.10994

773 Cipriani, A., Pretty, H., Hawton, K., Geddes, J.R., 2005. Lithium in the prevention of suicidal
774 behavior and all-cause mortality in patients with mood disorders: a systematic review of
775 randomized trials. Am. J. Psychiatry 162, 1805–1819. doi:10.1176/appi.ajp.162.10.1805

776 Corenthal, L.G., Boutt, D.F., Hynek, S.A., Munk, L.A., 2016. Regional groundwater flow and
777 accumulation of a massive evaporite deposit at the margin of the Chilean Altiplano.
778 Geophys. Res. Lett. 43, 8017–8025. doi:10.1002/2016GL070076

779 Cornellà, O., Salas, J., Aravena, R., Guzmán, E., Guimerà, J., Tore, C., Von Igel, W., Henríquez,
780 A., Fock, A., 2009. Hidrogeologia de los sistemas lagunares del margen E del Salar de
781 Atacama, in: XII Congreso Geológico Chileno. Santiago de Chile, pp. 1–4.

782 Custodio, E., Bruggeman, G.A., 1987. Groundwater problems in coastal areas. Studies and

783 reports in hydrology, UNESCO.

784 Diersch, H.-J.G., 2014. FEFLOW: Finite Element Modeling of Flow, Mass and Heat Transport in
785 Porous and Fractured Media. doi:10.1007/978-3-642-38739-5

786 Dirección General de Aguas, 2013. Análisis de la oferta hídrica del Salar de Atacama. Santiago,
787 Chile.

788 Dirección General de Aguas, 2010. Actualización de la evaluación de la disponibilidad de
789 recursos hídricos para constituir derechos de aprovechamientos en las subcuencas
790 afluentes al Salar de Atacama. II Región Informe final. Santiago, Chile.

791 Dirección General de Aguas, 1986. Balance Hidrologico Nacional II Region. Santiago, Chile.

792 Doherty, J., 2015. Calibration and Uncertainty Analysis for Complex Environmental Models.
793 Groundwater 56, 673–674.

794 Duffy, C.J., Al-Hassan, S., 1988. Groundwater circulation in a closed desert basin: Topographic
795 scaling and climatic forcing. Water Resour. Res. 24, 1675–1688.
796 doi:10.1029/WR024i010p01675

797 Evans, R.K., 1978. Lithium reserves and resoruces. Energy 3, 379–385.

798 Fan, Y., Duffy, C.J., Oliver, D.S., 1997. Density-driven groundwater flow in closed desert basins:
799 Field investigations and numerical experiments. J. Hydrol. 196, 139–184.
800 doi:10.1016/S0022-1694(96)03292-1

801 Ferguson, G., Gleeson, T., 2012. Vulnerability of coastal aquifers to groundwater use and
802 climate change. Nat. Clim. Chang. 2, 342–345. doi:10.1038/nclimate1413

803 Garreaud, R.D., Molina, A., Farias, M., 2010. Andean uplift, ocean cooling and Atacama
804 hyperaridity: A climate modeling perspective. Earth Planet. Sci. Lett. 292, 39–50.
805 doi:10.1016/j.epsl.2010.01.017

806 Godfrey, L. V., Chan, L.H., Alonso, R.N., Lowenstein, T.K., McDonough, W.F., Houston, J., Li, J.,
807 Bobst, A., Jordan, T.E., 2013. The role of climate in the accumulation of lithium-rich brine
808 in the central andes. Appl. Geochemistry 38, 92–102.
809 doi:10.1016/j.apgeochem.2013.09.002

810 Hamann, E., Post, V., Kohfahl, C., Prommer, H., Simmons, C.T., 2015. Numerical investigation of
811 coupled density-driven flow and hydrogeochemical processes below playas. Water
812 Resour. Res. 51, 9338–9352. doi:10.1002/2015WR017833

Hardie, L.A., 1991. On the significance of evaporites. Annu. Rev. Earth Planet. Sci. 19, 131–68.

Hartley, A.J., Chong, G., 2002. Late Pliocene age for the Atacama Desert: Implications for the desertification of western South America. Geology 30, 43–46. doi:10.1130/0091-7613(2002)030<0043:LPAFTA>2.0.CO;2

HARZA, 1978. Desarrollo de los recursos de agua en el Norte Grande, Chile. Santiago, Chile.

Herrera, C., Custodio, E., Chong, G., Lambán, L.J., Riquelme, R., Wilke, H., Jódar, J., Urrutia, J., Urqueta, H., Sarmiento, A., Gamboa, C., Lictevout, E., 2016. Groundwater flow in a closed basin with a saline shallow lake in a volcanic area: Laguna Tuyajto, northern Chilean Altiplano of the Andes. Sci. Total Environ. 541, 303–318. doi:10.1016/j.scitotenv.2015.09.060

Holzbecher, E., 2005. Groundwater flow pattern in the vicinity of a salt lake. Hydrobiologia 532, 233–242.

Houston, J., 2009. A recharge model for high altitude, arid, Andean aquifers. Hydrol. Process. 23, 2383–2393. doi:10.1002/hyp.7350

Houston, J., 2006. Variability of precipitation in the Atacama Desert: Its causes and hydrological impact. Int. J. Climatol. 26, 2181–2198. doi:10.1002/joc.1359

Huerta-Vásquez, G., 2012. Evaluation of Chemical Patterns in Brines in the Salar de Atacama , Northern Chile : A Chemical and Isotopic approach. University of Waterloo.

IDAEA-CSIC, 2017. Cuarta actualización del modelo hidrogeológico del Salar de Atacama. Santiago, Chile.

Jordan, T.E., Mpodozis, C., Muñoz, N., Blanco, N., Pananont, P., Gardeweg, M., 2007. Cenozoic subsurface stratigraphy and structure of the Salar de Atacama Basin, northern Chile. J. South Am. Earth Sci. 23, 122–146. doi:10.1016/j.jsames.2006.09.024

Kampf, S.K., Tyler, S.W., 2006. Spatial characterization of land surface energy fluxes and uncertainty estimation at the Salar de Atacama, Northern Chile. Adv. Water Resour. 29, 336–354. doi:10.1016/j.advwatres.2005.02.017

Kampf, S.K., Tyler, S.W., Ortiz, C.A., Muñoz, J.F., Adkins, P.L., 2005. Evaporation and land surface energy budget at the Salar de Atacama, Northern Chile. J. Hydrol. 310, 236–252. doi:10.1016/j.jhydrol.2005.01.005

Kesler, S.E., Gruber, P.W., Medina, P.A., Keoleian, G.A., Everson, M.P., Wallington, T.J., 2012.

Global lithium resources: Relative importance of pegmatite, brine and other deposits. Ore Geol. Rev. 48, 55–69. doi:10.1016/j.oregeorev.2012.05.006

Lusczynski, N.J., 1961. Head and Flow of Ground Water of Variable Density. J. Geophys. Res. 66, 4247–4256. doi:10.1029/JZ066i012p04247

Maas, C., Emke, M.J., 1989. Solving varying density groundwater problems with a single density computer program, in: 10th SWIM. Ghent, pp. 143–154.

Marazuela, M.A., Vázquez-Suñé, E., Custodio, E., Palma, T., García-Gil, A., Ayora, C., 2018. 3D mapping, hydrodynamics and modelling of the freshwater-brine mixing zone in salt flats similar to the Salar de Atacama (Chile). J. Hydrol. 561, 223–235. doi:10.1016/j.jhydrol.2018.04.010

Mardones, L., 1998. Flux et évolution des solutions salines dans les systèmes hydrologiques des salars d'Ascotan et d'Atacama. University of Paris.

Mardones, L., 1986. Características geológicas e hidrogeológicas del Salar de Atacama, in: Lagos, G. (Ed.), El Litio, Un Nuevo Recurso Para Chile. pp. 181–216.

Marom, R., Amalraj, S.F., Leifer, N., Jacob, D., Aurbach, D., 2011. A review of advanced and practical lithium battery materials. J. Mater. Chem. 21, 9938–9954. doi:10.1039/c0jm04225k

Mishra, S.K., Singh, V., 2003. Soil Conservation Service Curve Number (SCS-CN) Methodology. Springer Netherlands. doi:10.1007/978-94-017-0147-1

Mpodozis, C., Arriagada, C., Basso, M., Roperch, P., Cobbold, P., Reich, M., 2005. Late Mesozoic to Paleogene stratigraphy of the Salar de Atacama Basin, Antofagasta, Northern Chile: Implications for the tectonic evolution of the Central Andes. Tectonophysics 399, 125–154. doi:10.1016/j.tecto.2004.12.019

Munk, L.A., Hynek, S.A., Bradley, D., Boutt, D.F., Labay, K., Jochens, H., 2016. Lithium brines: A global perspective. Rev. Econ. Geol. 18, 339–365.

Muñoz-Pardo, J.F., Ortiz-Astete, C.A., Mardones-Pérez, L., de Vidts-Sabelle, P., 2004. Funcionamiento hidrogeológico del acuífero del núcleo del salar de Atacama, Chile. Ing. Hidráulica en Mex. XIX, 69–81.

Oude-Essink, G.H.P., 2001. Improving fresh groundwater supply—problems and solutions. Ocean Coast. Manag. 44, 429–449. doi:10.1016/S0964-5691(01)00057-6

873 Philip, J.R., 1957. Evaporation, and moisture and heat fields in the soil. J. Meteorol. 14, 354–
874 366. doi:10.1175/1520-0469(1957)014<0354:EAMAHF>2.0.CO;2

875 Post, V., Kooi, H., Simmons, C., 2007. Using hydraulic head measurements in variable-density
876 ground water flow analyses. Ground Water 45, 664–671. doi:10.1111/j.1745-
877 6584.2007.00339.x

878 Post, V.E.A., Groen, J., Kooi, H., Person, M., Ge, S., Edmunds, W.M., 2013. Offshore fresh
879 groundwater reserves as a global phenomenon. Nature 504, 71–78.
880 doi:10.1038/nature12858

881 Post, V.E.A., Werner, A.D., 2017. Coastal aquifers: Scientific advances in the face of global
882 environmental challenges. J. Hydrol. 551, 1–3. doi:10.1016/j.jhydrol.2017.04.046

883 Pueyo, J.J., Chong, G., Ayora, C., 2017. Lithium saltworks of the Salar de Atacama: A model for
884 MgSO4-free ancient potash deposits. Chem. Geol. 466, 173–186.
885 doi:10.1016/j.chemgeo.2017.06.005

886 Rech, J.A., Currie, B.S., Michalski, G., Cowan, A.M., 2006. Neogene climate change and uplift in
887 the Atacama Desert, Chile. Geology. doi:10.1130/G22444.1

888 Rio Chilex S.A, 1997. Evaluación hidrogeológica acuífero sector norte Salar de Atacama.
889 Santiago, Chile.

890 Risacher, F., Alonso, H., Salazar, C., 2003. The origin of brines and salts in Chilean salars: A
891 hydrochemical review. Earth-Science Rev. 63, 249–293. doi:10.1016/S0012-
892 8252(03)00037-0

893 Rissmann, C., Leybourne, M., Benn, C., Christenson, B., 2015. The origin of solutes within the
894 groundwaters of a high Andean aquifer. Chem. Geol. 396, 164–181.
895 doi:10.1016/j.chemgeo.2014.11.029

896 Rockwood-Lithium, 2015. Estudio Hidrogeológico y Modelo Numérico Sector Sur del Salar de
897 Atacama (Anexo 1). Para Estudio de Impacto Ambiental Proyecto Modificaciones y
898 Mejoramiento del Sistema de Pozas de Evaporación solar en el Salar de Atacama.
899 Santiago, Chile.

900 Rosen, M.R., 1994. The importance of groundwater in playas: A review of playa classifications
901 and the sedimentology and hydrology of playas. Geol. Soc. Am. Spec. Pap. 289, 1–18.
902 doi:10.1130/SPE289-p1

903 Salas, J., Guimerà, J., Cornellà, O., Aravena, R., Guzmán, E., Tore, C., Von Igel, W., Moreno, R.,
904 2010. Hidrogeologia del sistema lagunar del margen este del Salar de Atacama (Chile).
905 Bol. Geol. y Min. 121, 357–372.

906 Scanlon, B.R., Keese, K.E., Flint, A.L., Flint, L.E., Gaye, C.B., Edmunds, W.M., Simmers, I., 2006.
907 Global synthesis of groundwater recharge in semiarid and arid regions. Hydrol. Process.
908 20, 3335–3370. doi:10.1002/hyp.6335

909 Scanlon, B.R., Mace, R.E., Barrett, M.E., Smith, B., 2003. Can we simulate regional groundwater
910 flow in a karst system using equivalent porous media models? Case study, Barton Springs
911 Edwards aquifer, USA. J. Hydrol. 276, 137–158. doi:10.1016/S0022-1694(03)00064-7

912 Skrzypek, G., Mydłowski, A., Dogramaci, S., Hedley, P., Gibson, J.J., Grierson, P.F., 2015.
913 Estimation of evaporative loss based on the stable isotope composition of water using
914 Hydrocalculator. J. Hydrol. 523, 781–789. doi:10.1016/j.jhydrol.2015.02.010

915 Strack, O.D.L., 1976. A single-potential solution for regional interface problems in coastal
916 aquifers. Water Resour. Res. 12, 1165–1174. doi:10.1029/WR012i006p01165

917 Tarascon, J.-M., 2010. Is lithium the new gold? Nat. Chem. 2, 510–510. doi:10.1038/nchem.680

918 Tejeda, I., Cienfuegos, R., Muñoz, J.F., Durán, M., 2003. Numerical Modeling of Saline Intrusion
919 in Salar de Atacama. J. Hydrol. Eng. 8, 25–34. doi:10.1061/(ASCE)1084-0699(2003)8:1(25)

920 Tyler, S.W., Muñoz, J.F., Wood, W.W., 2006. The response of playa and sabkha hydraulics and
921 mineralogy to climate forcing. GroundwaterWater 44, 329–338. doi:10.1111/j.1745-
922 6584.2005.00096.x

923 Vásquez, C., Ortiz, C., Suárez, F., Muñoz, J.F., 2013. Modeling flow and reactive transport to
924 explain mineral zoning in the Atacama salt flat aquifer, Chile. J. Hydrol. 490, 114–125.
925 doi:10.1016/j.jhydrol.2013.03.028

926 Vikström, H., Davidsson, S., Höök, M., 2013. Lithium availability and future production
927 outlooks. Appl. Energy 110, 252–266. doi:10.1016/j.apenergy.2013.04.005

928 Warren, J.K., 2010. Evaporites through time: Tectonic, climatic and eustatic controls in marine
929 and nonmarine deposits. Earth-Science Rev. 98, 217–268.
930 doi:10.1016/j.earscirev.2009.11.004

931 Werner, A.D., Bakker, M., Post, V.E.A., Vandenbohede, A., Lu, C., Ataie-Ashtiani, B., Simmons,
932 C.T., Barry, D.A., 2013. Seawater intrusion processes, investigation and management:

933 Recent advances and future challenges. Adv. Water Resour. 51, 3–26.
934 doi:10.1016/j.advwatres.2012.03.004

935 Wood, W.W., Sanford, W.E., 1990. Ground-water control of evaporite deposition. Econ. Geol.
936 85, 1226–1235. doi:10.2113/gsecongeo.85.6.1226

937 Wooding, R.A., Tyler, S.W., White, I., 1997. Convection in groundwater below an evaporating
938 Salt Lake: 1. Onset of instability. Water Resour. Res. 33, 1199–1217.
939 doi:10.1029/96WR03533

940 XTERRAE, 2011. Modelo geológico del Salar de Atacama. Internal report of SQM.

941 Yechieli, Y., Wood, W.W., 2002. Hydrogeologic processes in saline systems: Playas, sabkhas,
942 and saline lakes. Earth-Science Rev. 58, 343–365. doi:10.1016/S0012-8252(02)00067-3

943

944

945

946

947

948

949

950

951

952

953

954

955

956

957

958

959 **FIGURE CAPTIONS**

960 **FIGURE 1**: Hydrodynamics of the mixing zone. IMZ - internal mixing zone; MMZ - middle mixing
961 zone; EMZ - external mixing zone. Modified from Marazuela et al. (2018).

962 **FIGURE 2**: Location of the SdA (LANDSAT 8, 27 September, 2016). The three sub-zones of the
963 mixing zone are shown in orange lettering (internal, IMZ, middle, MMZ and external, EMZ).

964 **FIGURE 3:** Type stratigraphic profile of the western salt flat nucleus. The blue letters highlight
965 the main hydrogeological units considered in the numerical model.

966 **FIGURE 4**: A) Isohyets map of the SdA basin. The white lines show the sub-basin zoning, and
967 the green triangles show the weather stations. B) Regional recharge sub-basins. The values of
968 each sub-basin are listed in Table 1. C) Recharge zones in the surface of the model domain. The
969 values of each sub-basin are listed in Table 2.

970 **FIGURE 5**: A) Zoning of hydraulic conductivity in aquifer A (KA). B) Zoning of hydraulic
971 conductivity in aquitard AB (KAB) and aquifer B (KB). The hydraulic conductivity values of each
972 zone are listed in Table S1.

973 **FIGURE 6:** Geometry of each of the geological surfaces that define aquifer A, aquitard AB and
974 aquifer B.

975 **FIGURE 7:** Three-dimensional mesh of the numerical model. A) Top view of the mesh. In yellow
976 is the vertical cross-section of Figures B and C. B) North-South vertical cross-section. C) East-
977 west vertical cross-section.

978 **FIGURE 8**: Hydrogeological behaviour of the SdA basin. Q is Quelana lake, SLS is the Soncor
979 lake system, Tb is Tebenquiche lake and SP is the San Pedro alluvial fan. The black lines show
980 the groundwater flow in the mixing zone. The vertical scale was deformed to better show the
981 main hydrogeological features.

982 **FIGURE 9:** Precipitation data of the Peine and Chaxa weather stations (see their locations in
983 Figure 4A) and their effect on the hydraulic heads of the observational points P1, P2 and P3
984 (see their location in Figure 2). The dashed black line shows the average detention value.

985 **FIGURE 10**: Map of hydraulic heads of aquifer A that results from the numerical model.

986 **FIGURE 11**: Calibration results of the numerical model. The average error ($\overline{E}$), root mean
987 square (RMS) and standard deviation (σ) are shown.

FIGURE 12: Three-dimensional hydraulic head contour map of the vertical cross-section showed in Figure 10. Black lines show the high velocity freshwater flow and dashed black lines show the slow velocity brine flow.

FIGURE 13: Water balance that results from the 3D numerical model.

FIGURE 14: Plot of the $\delta^{18}O$ and $\delta^{2}H$ values of the groundwater from the eastern SdA recharge area. Values are from Huerta-Vásquez (2012) and Rissmann et al. (2015). Also plotted is the Local Meteoric Water Line (LMWL) from Aravena et al. (1999), Local Ground and Spring Water Line (see several authors collected in Rissmann et al., 2015), and evaporation trend that was calculated according to Skrzypek et al. (2015).

FIGURE 1

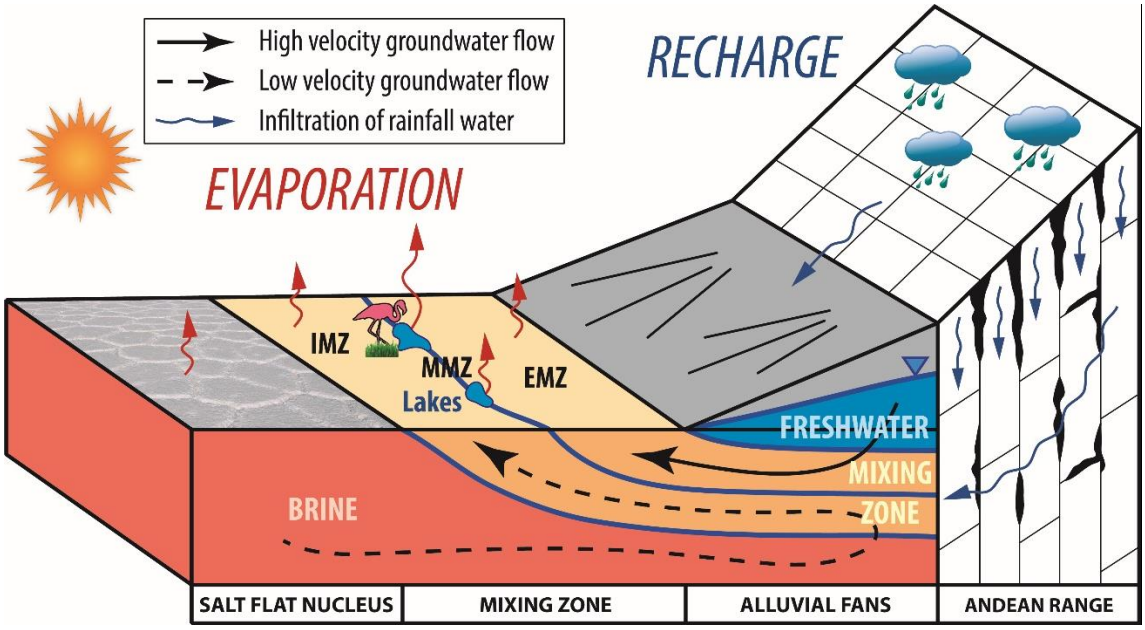
High velocity groundwater flow
Low velocity groundwater flow
Infiltration of rainfall water
RECHARGE
EVAPORATION
IMZ
MMZ
Lakes
EMZ
FRESHWATER
MIXING
ZONE
BRINE
SALT FLAT NUCLEUS
MIXING ZONE
ALLUVIAL FANS
ANDEAN RANGE

FIGURE 2

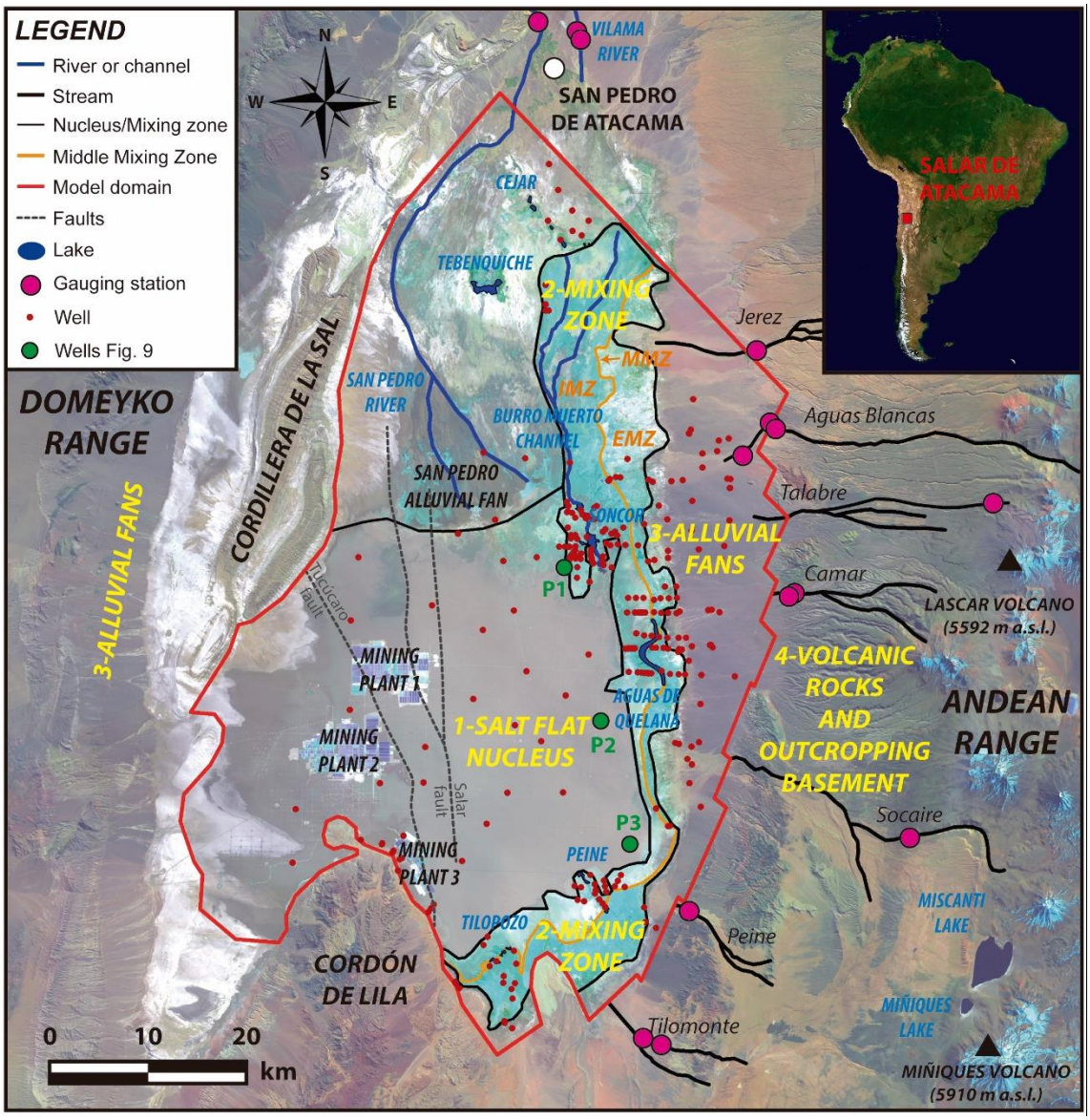
LEGEND
River or channel
Stream
Nucleus/Mixing zone
Middle Mixing Zone
Model domain
Faults
Lake
Gauging station
Well
Wells Fig. 9
N
W
E
S
VILAMA RIVER
SAN PEDRO DE ATACAMA
SALAR DE ATACAMA
CEJAR
TEBENQUICHE
2-MIXING ZONE
MMZ
IMZ
EMZ
Jerez
Aguas Blancas
Talabre
Camar
LASCAR VOLCANO (5592 m a.s.l.)
SAN PEDRO RIVER
BURRO MUERTO CHANNEL
SAN PEDRO ALLUVIAL FAN
CONCOR
3-ALLUVIAL FANS
P1
DOMEYKO RANGE
CORDILLERA DE LA SAL
3-ALLUVIAL FANS
Llucaro fault
MINING PLANT 1
MINING PLANT 2
MINING PLANT 3
AGUAS DE QUELANA
1-SALT FLAT NUCLEUS
P2
P3
Salar fault
4-VOLCANIC ROCKS AND OUTCROPPING BASEMENT
ANDEAN RANGE
Socaire
PEINE
TILOPOZO
2-MIXING ZONE
Peine
MISCANTI LAKE
MIÑIQUES LAKE
Tilomonte
MIÑIQUES VOLCANO (5910 m a.s.l.)
CORDÓN DE LILA
0
10
20
km

FIGURE 3

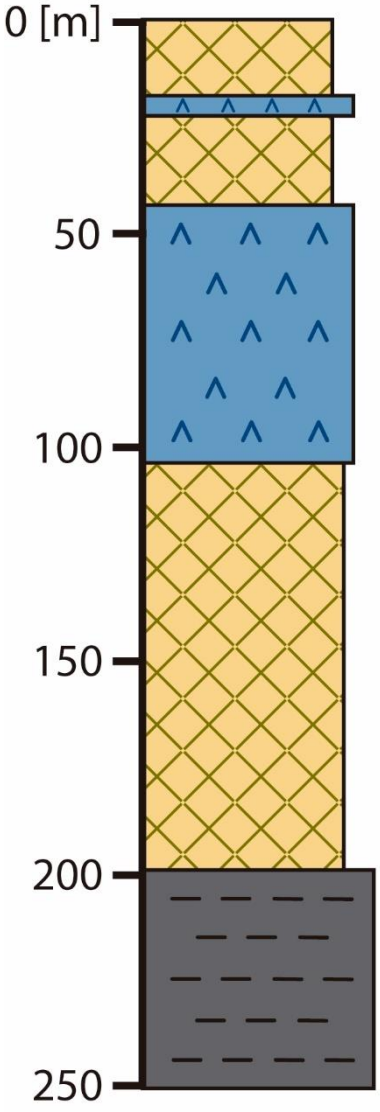

UNIT	DESCRIPTION
A	Upper halite
AB	Upper gypsum with carbonates
B	Middle halite
C	Middle gypsum
D	Lower halite
E	Clays

FIGURE 4

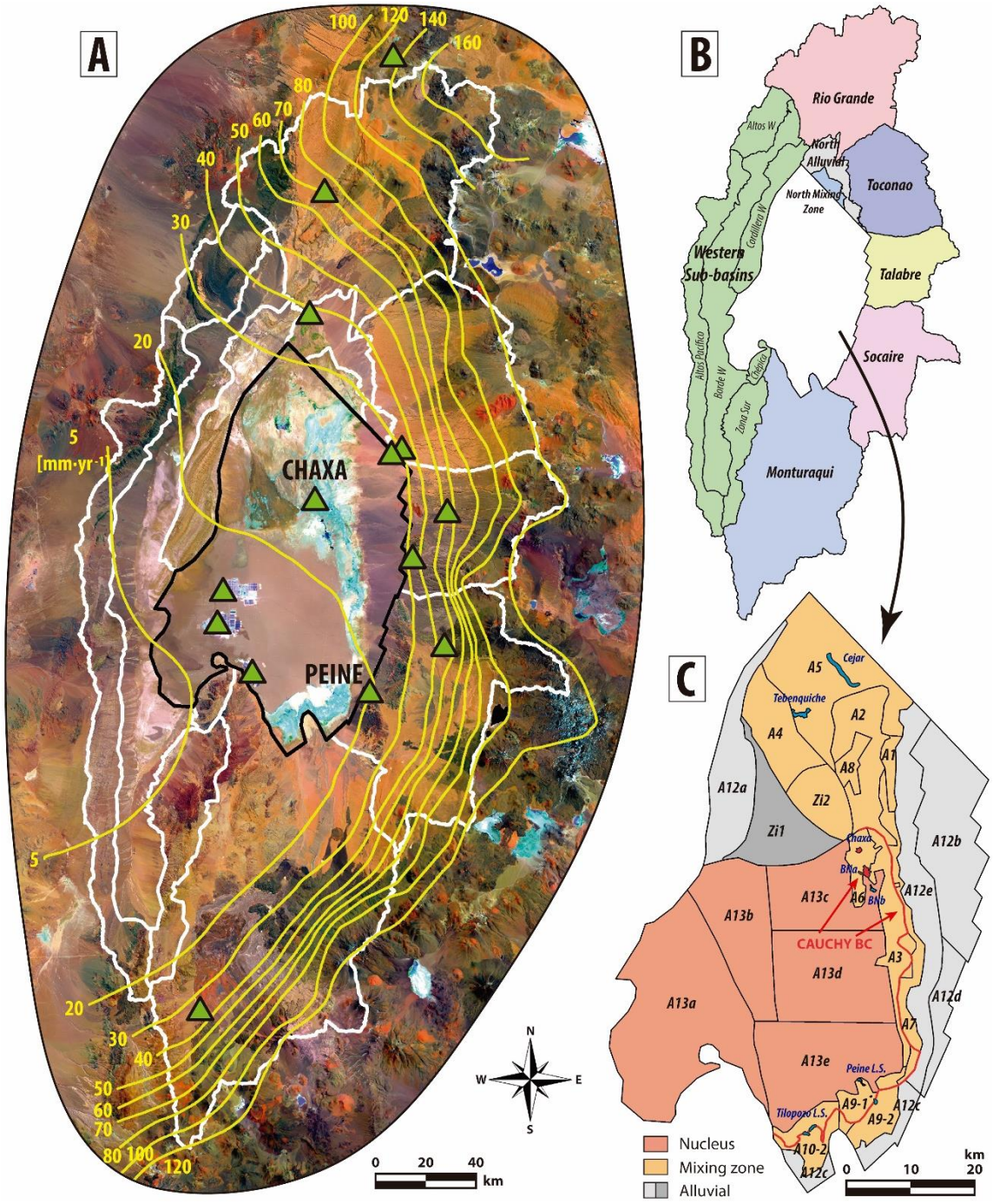
A
100
120
140
160
80
70
60
50
40
30
20
5
[mm·yr-1]
CHAXA
PEINE
N
W
E
S
0 20 40
km
B
Rio Grande
Altos W
North Alluvial
Toconao
North Mixed Zone
Cordillera W
Western Sub-basins
Talabre
Socaire
Altos Pacifico
Borde W
Chalviri
Zona Sur
Monturaqui
C
A5
Cejar
Tebenquiche
A2
A4
A8
A1
A12a
Zi2
Zi1
A12b
Chaxa
BNa
BNb
A6
A13c
A12e
A13b
CAUCHY BC
A3
A13d
A12d
A13a
A7
A13e
Peine L.S.
A9-1
A12c
Tilopozo L.S.
A9-2
A10-2
A12c
Nucleus
Mixing zone
Alluvial
0 10 20
km

FIGURE 5

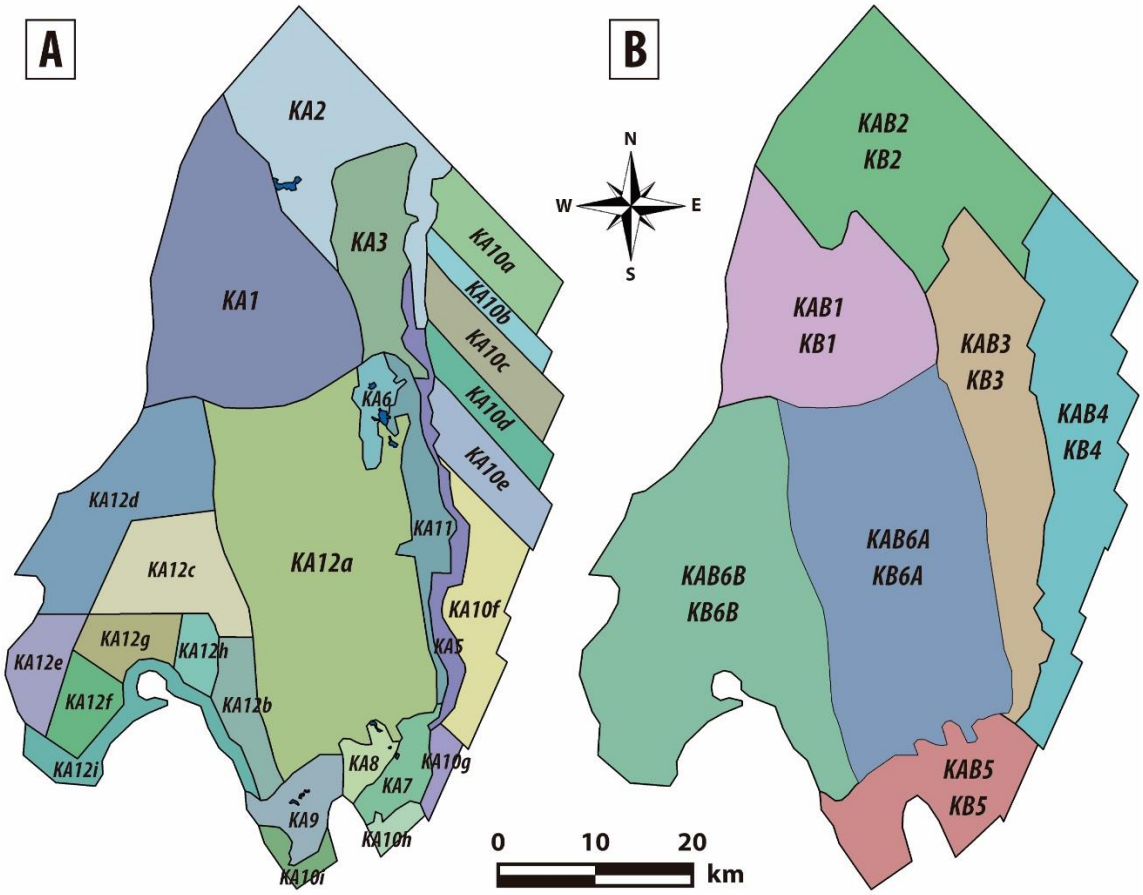
A
B
KA2
KA3
KA1
KA10a
KA10b
KA10c
KA10d
KA10e
KA6
KA12d
KA12c
KA12a
KA11
KA10f
KA5
KA12g
KA12h
KA12e
KA12f
KA12b
KA12i
KA8
KA7
KA10g
KA9
KA10h
KA10i
N
W
E
S
KAB2
KB2
KAB1
KB1
KAB3
KB3
KAB4
KB4
KAB6A
KB6A
KAB6B
KB6B
KAB5
KB5
0
10
20
km

FIGURE 6

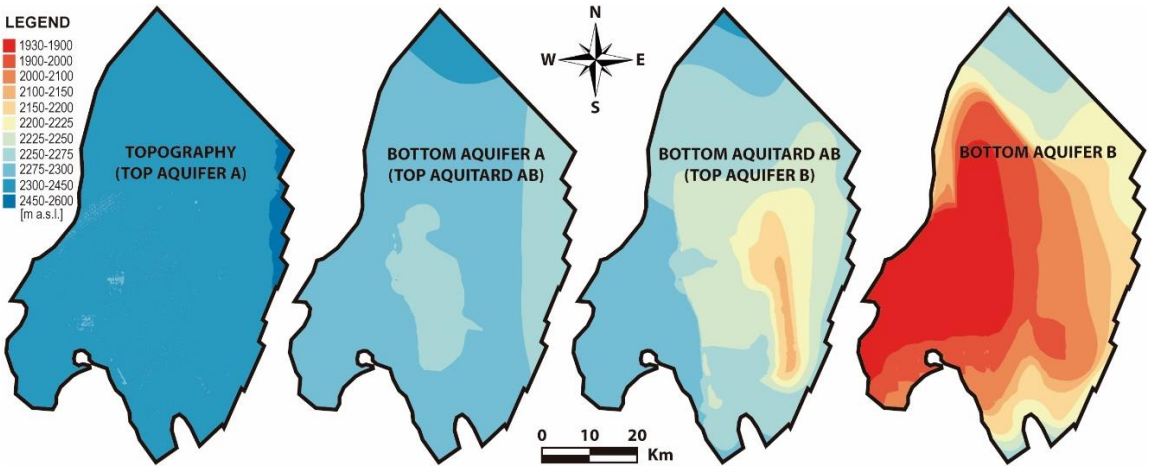
LEGEND
1930-1900
1900-2000
2000-2100
2100-2150
2150-2200
2200-2225
2225-2250
2250-2275
2275-2300
2300-2450
2450-2600
[m a.s.l.]
TOPOGRAPHY (TOP AQUIFER A)
BOTTOM AQUIFER A (TOP AQUITARD AB)
BOTTOM AQUITARD AB (TOP AQUIFER B)
BOTTOM AQUIFER B
N
W
E
S
0 10 20
Km

FIGURE 7

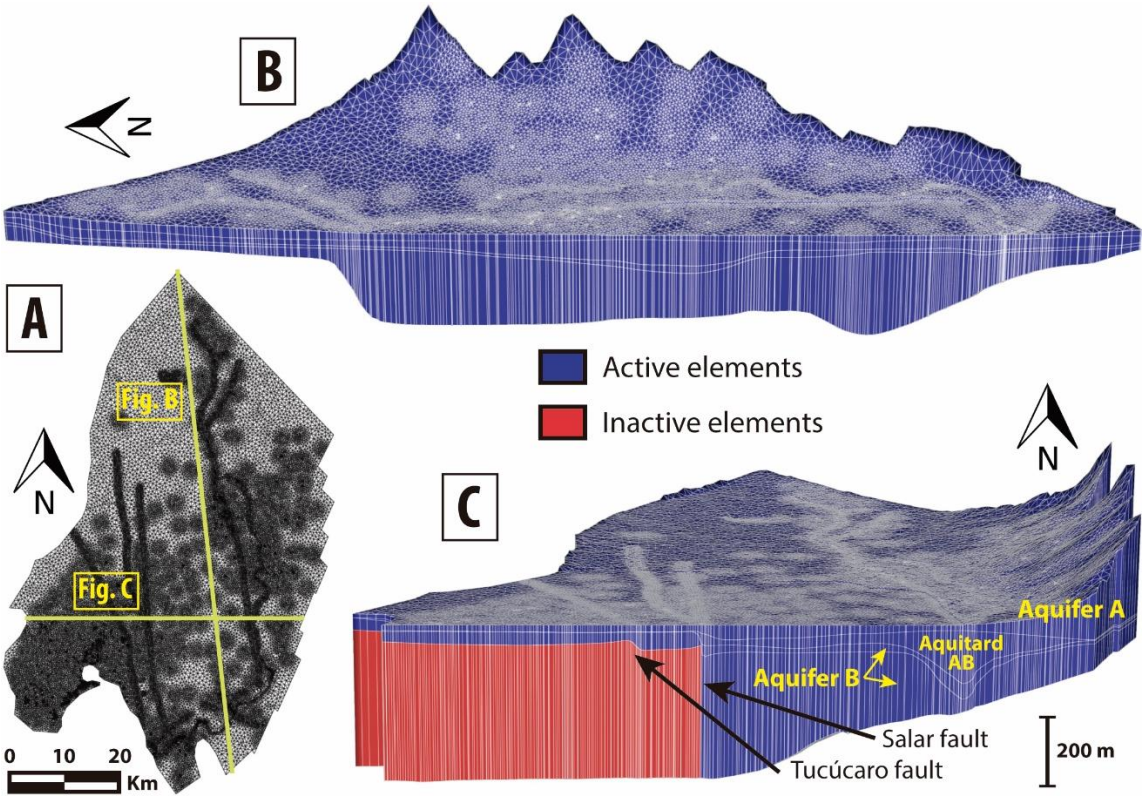
B
N
A
Fig. B
N
Fig. C
0 10 20
Km
Active elements
Inactive elements
C
N
Aquifer A
Aquitard AB
Aquifer B
Salar fault
Tucúcaro fault
200 m

FIGURE 8

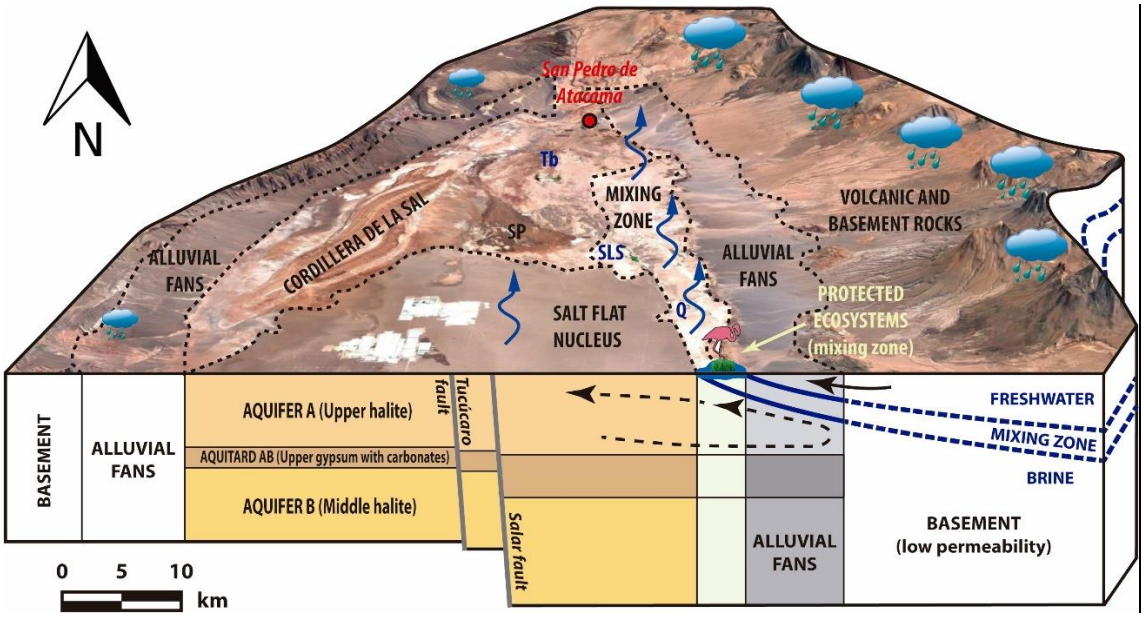
N
San Pedro de Atacama
Tb
MIXING ZONE
SP
SLS
Q
CORDILLERA DE LA SAL
ALLUVIAL FANS
SALT FLAT NUCLEUS
VOLCANIC AND BASEMENT ROCKS
ALLUVIAL FANS
PROTECTED ECOSYSTEMS (mixing zone)
BASEMENT
ALLUVIAL FANS
AQUIFER A (Upper halite)
AQUITARD AB (Upper gypsum with carbonates)
AQUIFER B (Middle halite)
Tucúcaro fault
Salar fault
ALLUVIAL FANS
FRESHWATER
MIXING ZONE
BRINE
BASEMENT (low permeability)
0 5 10
km

FIGURE 9

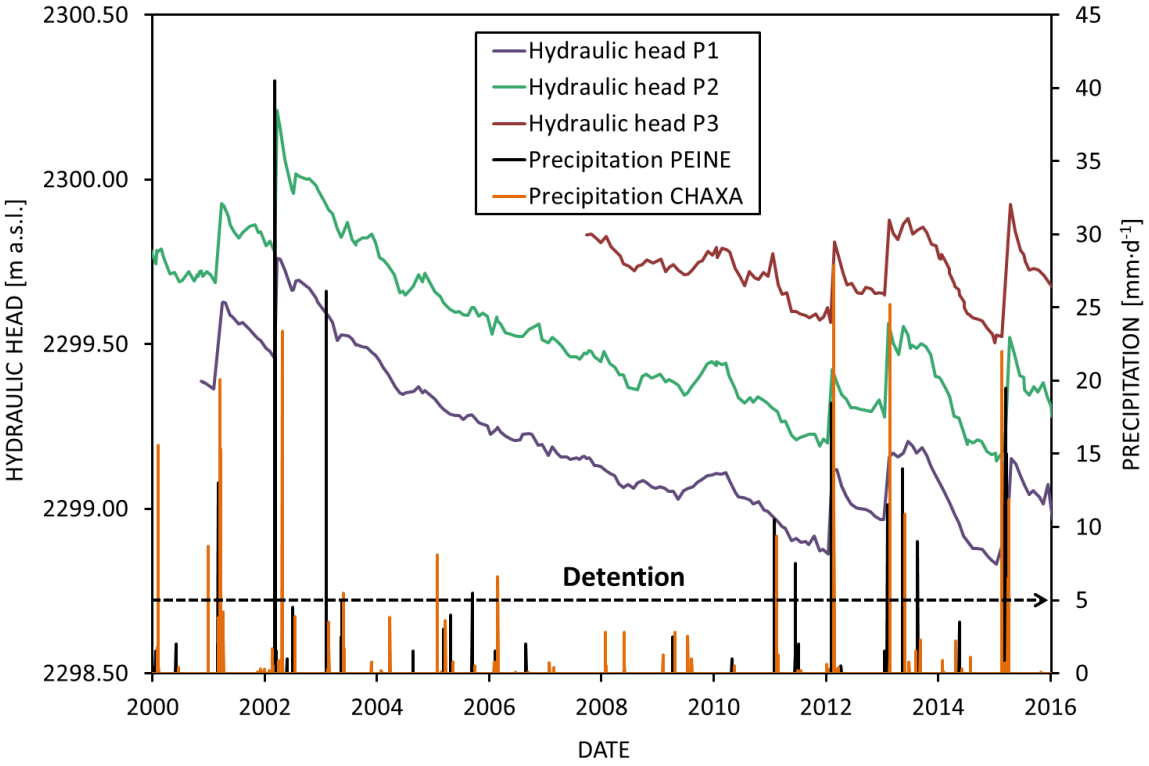
Hydraulic head P1
Hydraulic head P2
Hydraulic head P3
Precipitation PEINE
Precipitation CHAXA
Detention
HYDRAULIC HEAD [m a.s.l.]
PRECIPITATION [mm·d-1]
DATE
2300.50
2300.00
2299.50
2299.00
2298.50
45
40
35
30
25
20
15
10
5
0
2000
2002
2004
2006
2008
2010
2012
2014
2016

FIGURE 10

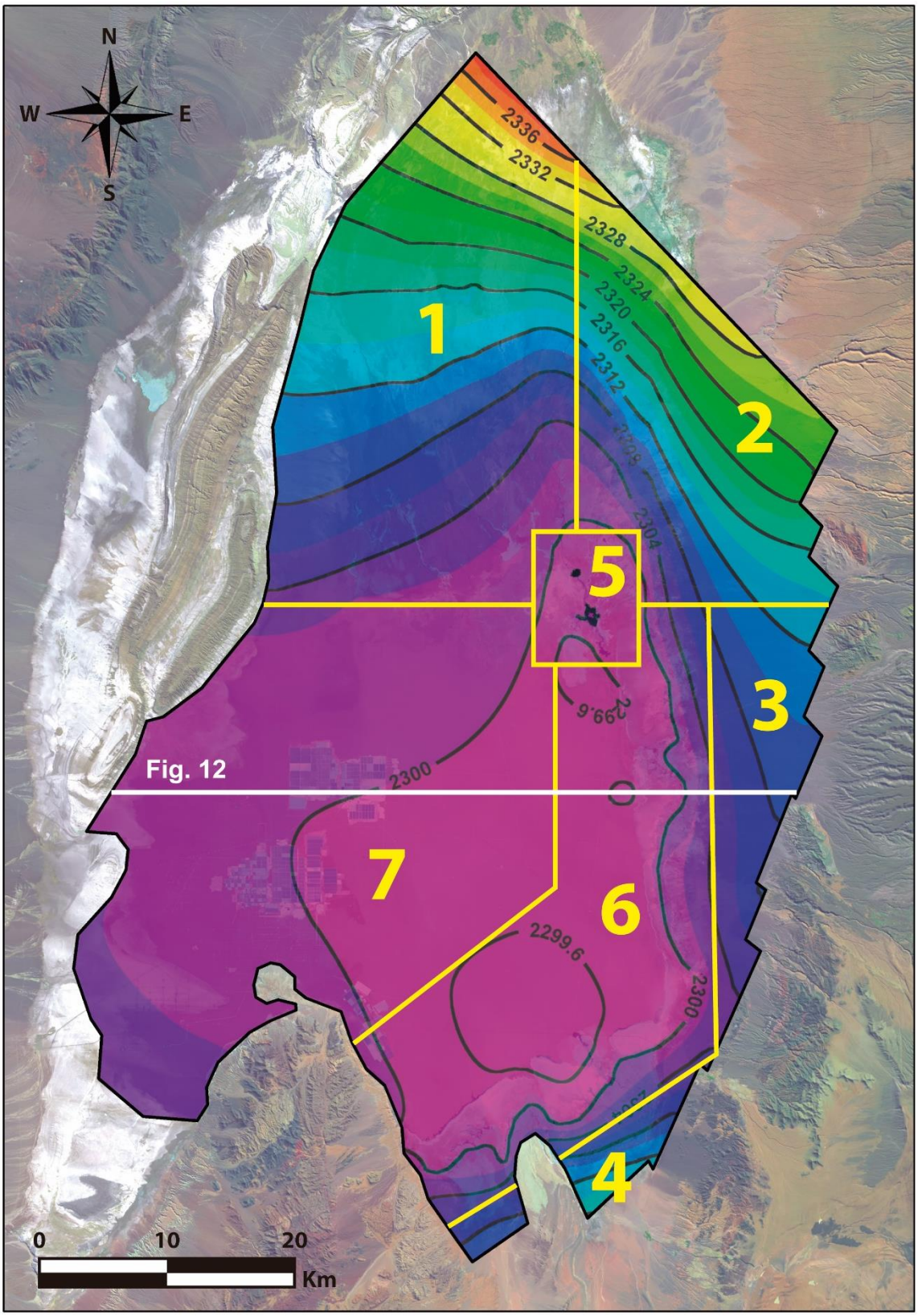
N
W
E
S
2336
2332
2328
2324
2320
2316
2312
2304
2300
2299.6
1
2
3
4
5
6
7
Fig. 12
0
10
20
Km

FIGURE 11

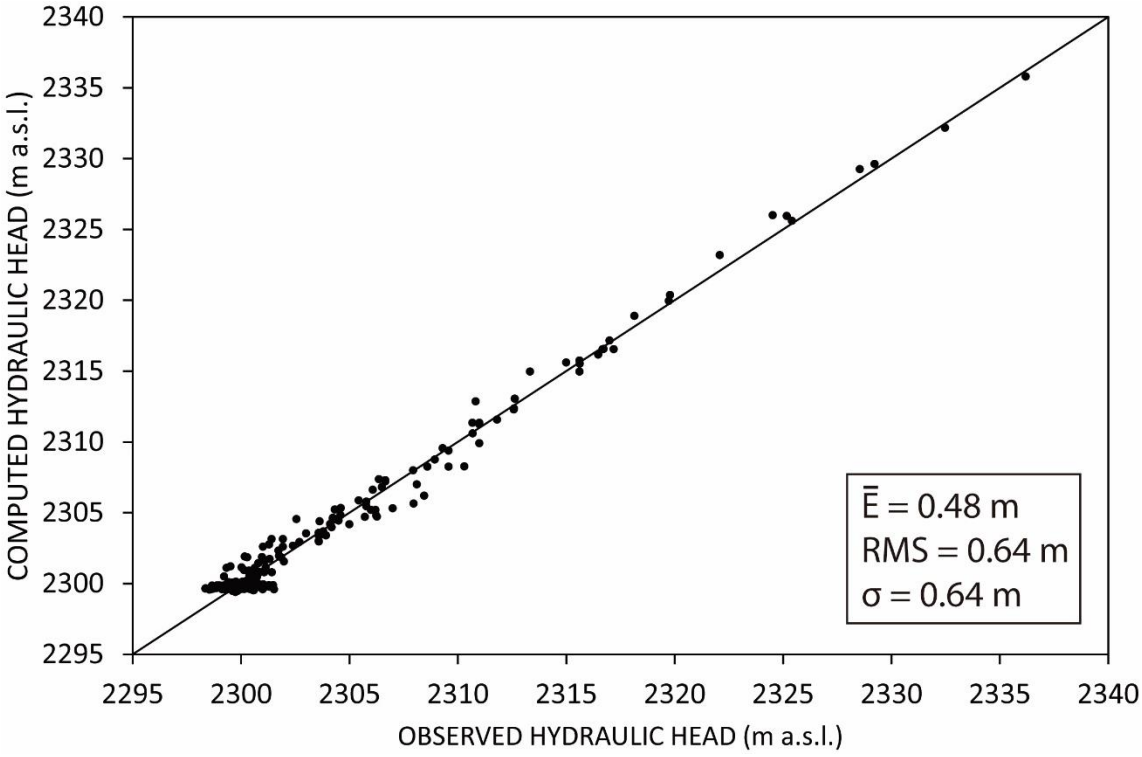
COMPUTED HYDRAULIC HEAD (m a.s.l.)
OBSERVED HYDRAULIC HEAD (m a.s.l.)
2295
2300
2305
2310
2315
2320
2325
2330
2335
2340
Ē = 0.48 m
RMS = 0.64 m
σ = 0.64 m

FIGURE 12

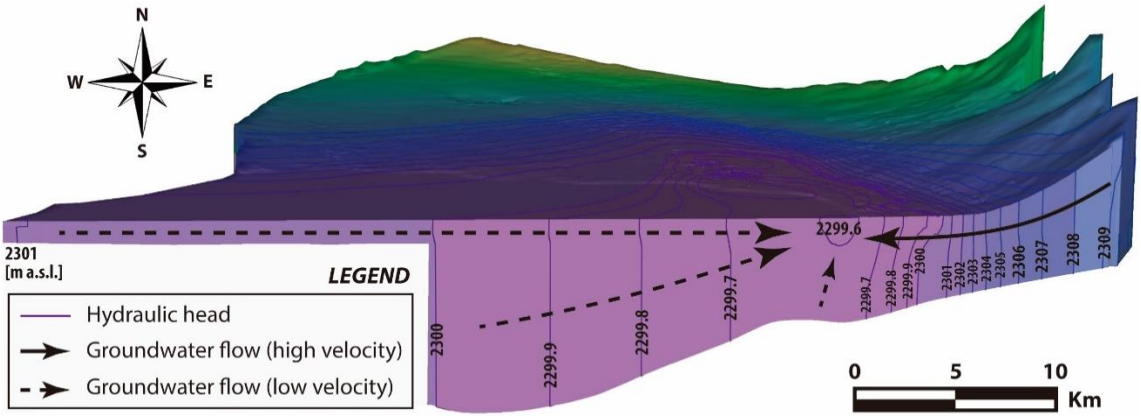
N
W
E
S
2301
[m a.s.l.]
LEGEND
Hydraulic head
Groundwater flow (high velocity)
Groundwater flow (low velocity)
2299.6
2300
2299.9
2299.8
2299.7
2301
2302
2303
2304
2305
2306
2307
2308
2309
0
5
10
Km

FIGURE 13

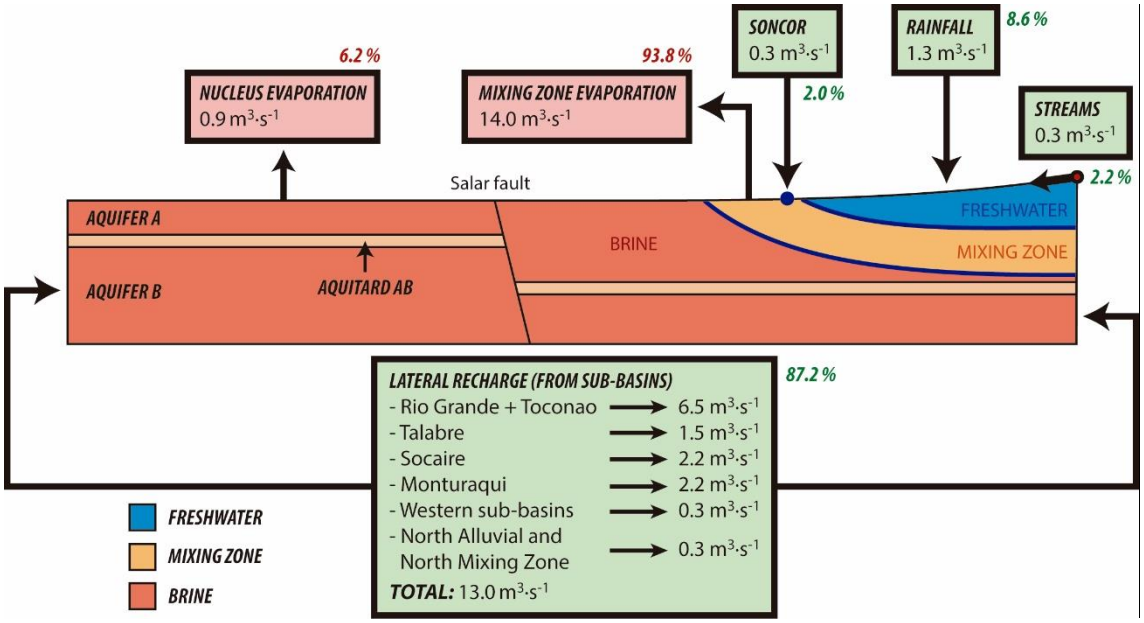
6.2 %
NUCLEUS EVAPORATION
0.9 m³·s⁻¹
93.8 %
MIXING ZONE EVAPORATION
14.0 m³·s⁻¹
SONCOR
0.3 m³·s⁻¹
2.0 %
RAINFALL
1.3 m³·s⁻¹
8.6 %
STREAMS
0.3 m³·s⁻¹
2.2 %
Salar fault
AQUIFER A
AQUIFER B
AQUITARD AB
BRINE
FRESHWATER
MIXING ZONE
87.2 %
LATERAL RECHARGE (FROM SUB-BASINS)
- Rio Grande + Toconao → 6.5 m³·s⁻¹
- Talabre → 1.5 m³·s⁻¹
- Socaire → 2.2 m³·s⁻¹
- Monturaqui → 2.2 m³·s⁻¹
- Western sub-basins → 0.3 m³·s⁻¹
- North Alluvial and North Mixing Zone → 0.3 m³·s⁻¹
TOTAL: 13.0 m³·s⁻¹
FRESHWATER
MIXING ZONE
BRINE

FIGURE 14

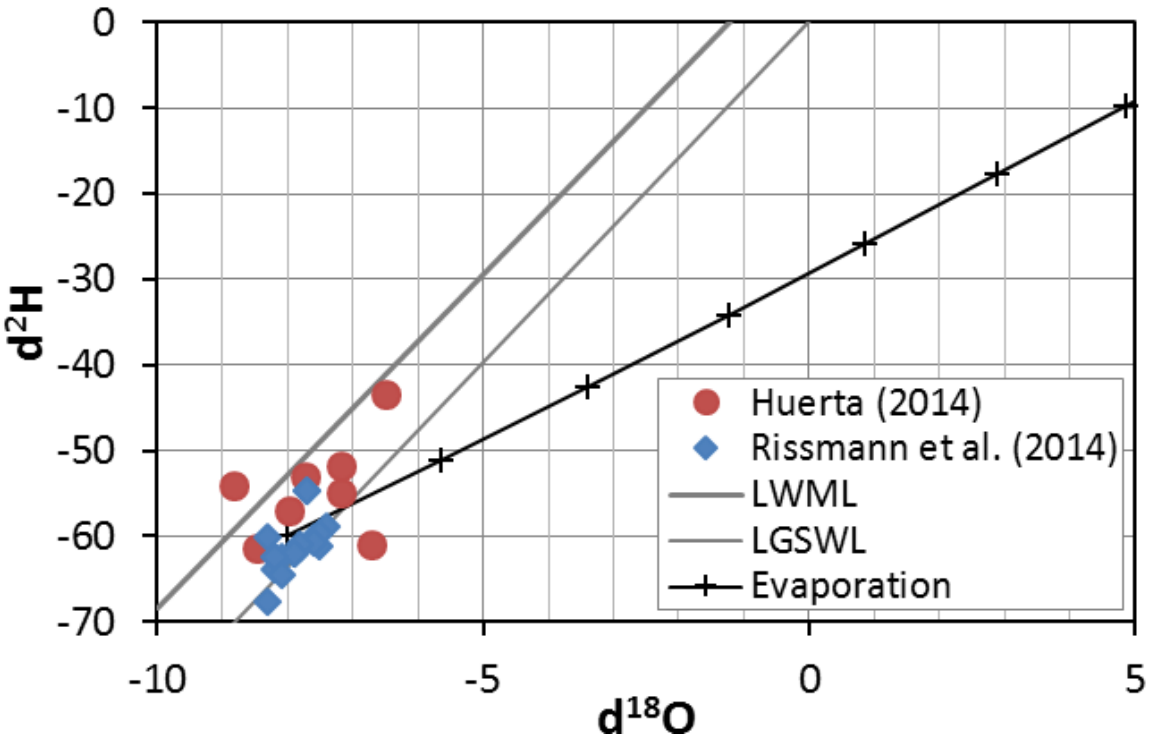
0
-10
-20
-30
-40
-50
-60
-70
d²H
-10
-5
0
5
d¹⁸O
Huerta (2014)
Rissmann et al. (2014)
LWML
LGSWL
Evaporation

TABLES

TABLE 1: Rainfall and recharge values for each sub-basin. The estimated and calibrated values are shown for the recharge. The sub-basin locations are shown in Figure 4B.

TABLE 2: Rainfall, recharge and evaporation values for each zone of the model domain. The recharge zones locations are shown in Figure 4C.

TABLE 3: Location (Coordinates in Universal Transverse Mercator, UTM) and flow of each stream.

TABLE 1

SUB-BASIN	AREA [km^2]	RAINFALL [$mm \cdot yr^{-1}$]	RAINFALL [$m^3 \cdot s^{-1}$]	DETENTION [%]	ESTIMATED RECHARGE [$m^3 \cdot s^{-1}$]	CALIBRATED RECHARGE [$m^3 \cdot s^{-1}$]
Rio Grande	2165	95	6.54	25	4.91	6.50
Toconao	1263	77	3.07	25	2.30	
Talabre	845	74	1.97	25	1.48	1.48
Socaire	1574	60	2.97	25	2.23	2.23
Monturaqui	3378	44	4.68	25	3.51	2.15
Altos Pacífico	1093	9	0.30	85	0.05	0.31
Altos W	354	37	0.41	85	0.06	
Borde W	1575	13	0.66	85	0.10	
Cordillera W	515	24	0.40	85	0.06	
Chépica	91	6	0.02	85	<0.01	
Zona Sur	521	9	0.15	85	0.02	
North Alluvial	279	35	0.31	35	0.20	0.25
North Mixing Zone	83	30	0.08	35	0.05	

TABLE 2

ZONE	SUB-ZONE	AREA [km²]	RAINFALL [mm·yr⁻¹]	RAINFALL [m³·s⁻¹]	DETENTION [%]	RECHARGE [m³·s⁻¹]	EVAPORATION [mm·yr⁻¹]		EVAPORATION [m³·s⁻¹]	
							Initial	*Calibrated*	*Initial*	*Calibrated*
Alluvial Zone	A12a	162	23	0.12	35	0.08	1	1	0.01	0.01
	A12b	274	24	0.21	35	0.14	0	0	0.00	0.00
	A12c	61	16	0.03	35	0.02	0	0	0.00	0.00
	A12d	57	23	0.04	35	0.03	0	0	0.00	0.00
	A12e	202	22	0.14	35	0.09	1	1	0.01	0.01
Mixing Zone	A1	21	24	0.02	35	0.01	97	113	0.06	0.07
	A2	127	25	0.10	35	0.07	1066	825	4.31	3.33
	A3	90	21	0.06	35	0.04	744	213	2.12	0.61
	A4	114	25	0.09	35	0.06	97	113	0.35	0.41
	A5	268	28	0.23	35	0.15	97	112	0.82	0.96
	A6	34	22	0.02	35	0.02	1066	514	1.16	0.56
	A7	71	21	0.05	35	0.03	97	764	0.22	1.72
	A8	25	25	0.02	35	0.01	1066	952	0.83	0.75
	A9-1	29	14	0.01	35	0.01	1355	174	1.27	0.16
	A9-2	51	16	0.03	35	0.02	1066	411	1.73	0.67
	A10-2	63	11	0.02	35	0.01	744	172	1.49	0.35
	BNa	1	21	0.00	35	0.00	2190	2190	0.09	0.09
	BNb	1	21	0.00	35	0.00	2190	2190	0.03	0.03
	Chaxa	1	22	0.00	35	0.00	2190	2190	0.02	0.02
	Tebenquiche	2	26	0.00	35	0.00	2190	2190	0.14	0.14
	Cejar	1	26	0.00	35	0.00	2190	2190	0.02	0.02
	Peine	1	16	0.00	35	0.00	2190	2190	0.05	0.05
	Tilopozo	1	11	0.00	35	0.00	2190	2190	0.03	0.03
Salt Flat Nucleus	A13a	507	8	0.13	35	0.09	20	20	0.33	0.33
	A13b	210	16	0.11	35	0.07	20	20	0.14	0.14
	A13c	178	20	0.11	35	0.07	20	20	0.11	0.11
	A13d	260	18	0.14	35	0.09	20	20	0.17	0.17
	A13e	273	14	0.12	35	0.08	20	20	0.18	0.18
	Zi1	140	22	0.10	35	0.06	0	7	0.00	0.03
	Zi2	78	23	0.06	35	0.04	2	8	0.01	0.02

TABLE 3

RIVER or STREAM	UTM East	UTM North	FLOW [$m^3 \cdot s^{-1}$]
San Pedro river	582083	7475499	0.72
Vilama river	583595	7470601	0.28
Jerez stream	602845	7435114	0.06
Aguas Blancas stream	600733	7425563	0.09
Talabre stream	623250	7420102	0.01
Camar	606284	7411161	0.01
Socaire stream	617452	7387854	0.15
Peine stream	596005	7380506	0.01
Tilomonte stream	590688	7368361	0.04

SUPPLEMENTARY MATERIAL

TABLE S1: Hydraulic conductivity values, both initially and calibrated by the numerical model. The location of each zone is shown in Figure 7.

1310

TABLE S1

UNIT	DOMAIN	ZONE	HYDRAULIC CONDUCTIVITY [m·d^{-1}]	
			REFERENCE VALUE	CALIBRATED
AQUIFER A	Mixing Zone	KA1	100	80
		KA2	100	220
		KA3	100	150
		KA4	100	200
		KA5	100	60
		KA6	100	300
		KA7	100	225
		KA8	100	190
		KA9	100	190
		KA11	100	190
		Lakes	10000	10000
	Alluvial Zone	KA10a	100	100
		KA10b	100	80
		KA10c	100	80
		KA10d	100	80
		KA10e	100	80
		KA10f	100	80
		KA10g	100	200
		KA10h	100	300
		KA10i	100	250
	Salt flat Nucleus	KA12a	200	300
		KA12b	200	140
		KA12c	200	160
		KA12d	200	160
		KA12e	200	100
		KA12f	200	100
		KA12g	200	100
		KA12h	200	140
		KA12i	200	140
AQUITARD AB	Mixing Zone	KAB-1	0.1	0.01
		KAB-2	1	2
		KAB-3	1	5
		KAB-4	1	2
		KAB-5	1	5
	Salt flat Nucleus	KAB-6	0.1	0.01
AQUIFER B	Mixing Zone	KB-1	1	1
		KB-2	10	20
		KB-3	10	20
		KB-4	10	20
		KB-5	10	20
	Salt flat Nucleus	KB-6	1	0.1

1311